A hot Saturn orbiting an oscillating late subgiant discovered by TESS

Huber, Daniel; Chaplin, William J.; Chontos, Ashley; Kjeldsen, Hans; Christensen-Dalsgaard, Joergen; Bedding, Timothy R.; Ball, Warrick; Brahm, Rafael; Espinoza, Nestor; Henning, Thomas; Jordan, Andres; Sarkis, Paula; Knudstrup, Emil; Albrecht, Simon; Grundahl, Frank; Andersen, Mads Fredslund; Palle, Pere L.; Crossfield, Ian; Fulton, Benjamin; Howard, Andrew W.

Document Version
Peer reviewed version

Citation for published version (Harvard):
Huber, D, Chaplin, WJ, Chontos, A, Kjeldsen, H, Christensen-Dalsgaard, J, Bedding, TR, Ball, W, Brahm, R, Espinoza, N, Henning, T, Jordan, A, Sarkis, P, Knudstrup, E, Albrecht, S, Grundahl, F, Andersen, MF, Palle, PL, Crossfield, I, Fulton, B, Howard, AW, Isaacson, HT, Weiss, LM, Handberg, R, Lund, MN, Serenelli, AM, Mosumgaard, J, Stokholm, A, Bierlya, A, Buchhave, LA, Latham, DW, Quinn, SN, Gaidos, E, Hirano, T, Ricker, GR, Vanderspek, RK, Seager, S, Jenkins, JM, Winn, JN, Antia, HM, Appourchaux, T, Basu, S, Bell, KJ, Benomar, O, Bonanno, A, Buzasi, DL, Campante, TL, Orhan, ZC, Corsaro, E, Cunha, MS, Davies, GR, Deheuvels, S, Grunblatt, SK, Hasanzadeh, A, Mauro, MPD, Garcia, RA, Gaulme, P, Girardi, L, Guzik, JA, Hon, M, Jiang, C, Kallinger, T, Kawaler, SD, Kuszlewicz, JS, Lebreton, Y, Li, T, Lucas, M, Lundkvist, MS, Mathis, S, Mathur, S, Mazumdar, A, Metcalfe, TS, Miglio, A, Monteiro, MJ, Mosser, B, Noll, A, Nsamba, B, Mann, AW, Ong, JMJ, Ortel, S, Pereira, F, Ranadive, P, Regulo, C, Rodrigues, TS, Roxburgh, IW, Aguirre, VS, Smalley, B, Schofield, M, Sousa, SG, Stassun, KG, Stello, D, Tayar, J, White, TR, Verma, K, Vrard, M, Yildiz, M, Baker, D, Bazot, M, Beichmann, C, Bergmann, C, Bugnet, L, Cale, B, Carlino, R, Cartwright, SM, Christiansen, JL, Ciardi, DR, Creevey, O, Dittmann, JA, Nascimento, JDD, Eylen, VV, Furesz, G, Gagne, J, Gao, P, Gazeas, K, Giddens, F, Hall, O, Hekker, S, Ireland, MJ, Latouf, N, LeBrun, D, Levine, AM, Matzko, W, Natinsky, E, Page, E, Plavchan, P, Mansouri-Samani, M, McCauliff, S, Mullally, SE, Orenstein, B, Soto, A, Paegert, M, Saders, JLV, Schnaible, C, Soderblom, DR, Szabo, R, Tanner, A, Tinney, CG, Teske, J, Thomas, A, Trampedach, R, Wright, D, Yuan, TT & Zohrabi, F 2019, 'A hot Saturn orbiting an oscillating late subgiant discovered by TESS', *The Astronomical Journal*, vol. 157, no. 6, 245. https://doi.org/10.3847/1538-3881/ab1488

[Link to publication on Research at Birmingham portal](#)

A HOT SATURN ORBITING AN OSCILLATING LATE SUBGIANT DISCOVERED BY TESS

Daniel Huber,[1] William J. Chaplin,[2,3] Ashley Chontos,[1,4] Hans Kjeldsen,[3,5] Jørgen Christensen-Dalsgaard,[3]
Timothy R. Bedding,[6,3] Warrick Ball,[2,3] Rafael Brahm,[7,8,9] Nestor Espinoza,[10] Thomas Henning,[10]
Andrés Jordán,[8,9] Paula Sarkis,[10] Emil Knudstrup,[3] Simon Albrecht,[3] Frank Grundahl,[3,5]
Mads Fredslund Andersen,[3] Pere L. Pallé,[11,12] Ian Crossfield,[13] Benjamin Fulton,[14] Andrew W. Howard,[15]
Howard T. Isaacson,[16] Lauren M. Weiss,[1] Rasmus Handberg,[3] Mikkel N. Lund,[3] Aldo M. Serenelli,[17,18]
Jakob Rørsted Mosumgaard,[3] Amalie Stokholm,[3] Allyson Bieryla,[19] Lars A. Buchhave,[20] David W. Latham,[19]
Samuel N. Quinn,[19] Eric Gaidos,[21] Teruyuki Hirano,[22,1] George R. Ricker,[13] Roland K. Vanderspek,[13]
Sara Seager,[13,23,24] Jon M. Jenkins,[25] Joshua N. Winn,[26] H. M. Antia,[27] Thierry Appourchaux,[28] Sarbani Basu,[29]
Keaton J. Bell,[30,3] Othman Benomar,[31] Alfio Bonanno,[32] Derek L. Buzasi,[33] Tiago L. Campante,[34,35]
Z. Çelik Orhan,[36] Enrico Corsaro,[32] Margarida S. Cunha,[34] Guy R. Davies,[2,3] Sebastien Deheuvels,[37]
Samuel K. Grunblatt,[1] Amir Hasanzadeh,[38] Maria Pia Di Mauro,[39] Rafael A. García,[40,41] Patrick Gaulme,[30,3]
Léo Girardi,[42] Joyce A. Guzik,[43] Marc Hon,[44] Chen Jiang,[45] Thomas Kallinger,[46] Steven D. Kawaler,[47]
James S. Kuszlewicz,[30,3] Yveline Lebreton,[48,49] Tanda Li,[6,3] Miles Lucas,[47] Mia S. Lundkvist,[3,50]
Andrew W. Mann,[51] Stéphane Mathis,[40,41] Savita Mathur,[11,12] Anwesh Mazumdar,[52] Travis S. Metcalfe,[53,54]
Andrea Miglio,[2,3] Mário J. P. F. G. Monteiro,[34,35] Benoit Mosser,[48] Anthony Noll,[37] Benard Nsamba,[34,35]
Jia Mian Joel Ong,[29] S. Örtel,[36] Filipe Pereira,[34,35] Pritesh Ranadive,[52] Clara Régulo,[11,12]
Thaíse S. Rodrigues,[42] Ian W. Roxburgh,[55] Victor Silva Aguirre,[3] Barry Smalley,[56] Mathew Schofield,[2,3]
Sérgio G. Sousa,[34] Keivan G. Stassun,[57,58] Dennis Stello,[44,6,3] Jamie Tayar,[1,59] Timothy R. White,[60]
Kuldeep Verma,[3] Mathieu Vrard,[34] M. Yildiz,[36] David Baker,[61] Michaël Bazot,[31] Charles Beichmann,[62]
Christoph Bergmann,[63] Lisa Bugnet,[40,41] Bryson Cale,[64] Roberto Carlino,[65] Scott M. Cartwright,[66]
Jessie L. Christiansen,[62] David R. Ciardi,[62] Orlagh Creevey,[67] Jason A. Dittmann,[19]
Jose-Dias Do Nascimento Jr.,[19,68] Vincent Van Eylen,[26] Gabor Fürész,[13] Jonathan Gagné,[69] Peter Gao,[16]
Kosmas Gazeas,[70] Frank Giddens,[71] Oliver J. Hall,[2,3] Saskia Hekker,[30,3] Michael J. Ireland,[60]
Natasha Latouf,[64] Danny LeBrun,[64] Alan M. Levine,[13] William Matzko,[64] Eva Natinsky,[61] Emma Page,[61]
Peter Plavchan,[64] Masoud Mansouri-Samani,[65] Sean McCauliff,[72] Susan E. Mullally,[73] Brendan Orenstein,[60]
Aylin Garcia Soto,[23] Martin Paegert,[19] Jennifer L. van Saders,[1] Chloe Schnaible,[61] David R. Soderblom,[73]
Róbert Szabó,[74,75] Angelle Tanner,[76] C. G. Tinney,[63] Johanna Teske,[69,77,59] Alexandra Thomas,[2,3]
Regner Trampedach,[53,3] Duncan Wright,[78] Thomas T. Yuan,[61] and Farzaneh Zohrabi[76]

[1] Institute for Astronomy, University of Hawai'i, 2680 Woodlawn Drive, Honolulu, HI 96822, USA

[2] School of Physics and Astronomy, University of Birmingham, Birmingham B15 2TT, UK

[3] Stellar Astrophysics Centre (SAC), Department of Physics and Astronomy, Aarhus University, Ny Munkegade 120, DK-8000 Aarhus C, Denmark

[4] NSF Graduate Research Fellow

[5] Institute of Theoretical Physics and Astronomy, Vilnius University, Sauletekio av. 3, 10257 Vilnius, Lithuania

[6] Sydney Institute for Astronomy (SIfA), School of Physics, University of Sydney, NSW 2006, Australia

[7] Center of Astro-Engineering UC, Pontificia Universidad Católica de Chile, Av. Vicuña Mackenna 4860, 7820436 Macul, Santiago, Chile

[8] Instituto de Astrofísica, Facultad de Física, Pontificia Universidad Católica de Chile

[9] Millennium Institute of Astrophysics, Av. Vicuña Mackenna 4860, 782-0436 Macul, Santiago, Chile

[10] Max-Planck-Institut fur Astronomie, Königstuhl 17, D-69117 Heidelberg, Germany

[11] Instituto de Astrofísica de Canarias (IAC), 38205 La Laguna, Tenerife, Spain

[12] Universidad de La Laguna (ULL), Departamento de Astrofísica, E-38206 La Laguna, Tenerife, Spain

[13] Department of Physics, and Kavli Institute for Astrophysics and Space Research, Massachusetts Institute of Technology, 77 Massachusetts Ave., Cambridge, MA 02139, USA

[14] NASA Exoplanet Science Institute / Caltech-IPAC, Pasadena, CA 91125, USA

[15] California Institute of Technology, Pasadena, CA 91125, USA

[16] Department of Astronomy, UC Berkeley, Berkeley, CA 94720, USA

[17] Institute of Space Sciences (ICE, CSIC) Campus UAB, Carrer de Can Magrans, s/n, E-08193, Barcelona, Spain

[18] Institut dEstudis Espacials de Catalunya (IEEC), C/Gran Capita, 2-4, E-08034, Barcelona, Spain

[19] Center for Astrophysics | Harvard & Smithsonian, 60 Garden St., Cambridge, MA 02138, USA

[20] DTU Space, National Space Institute, Technical University of Denmark, Elektrovej 328, DK-2800 Kgs. Lyngby, Denmark

huberd@hawaii.edu

arXiv:1901.01643v2 [astro-ph.EP] 5 Apr 2019

[21] Department of Earth Sciences, University of Hawaii at Mānoa, Honolulu, Hawaii 96822, USA

[22] Department of Earth and Planetary Sciences, Tokyo Institute of Technology, 2-12-1 Ookayama, Meguro-ku, Tokyo 152-8551, Japan

[23] Department of Earth, Atmospheric, and Planetary Sciences, Massachusetts Institute of Technology, 77 Massachusetts Ave., Cambridge, MA 02139, USA

[24] Department of Aeronautics and Astronautics, Massachusetts Institute of Technology, 77 Massachusetts Ave., Cambridge, MA 02139, USA

[25] NASA Ames Research Center, Moffett Field, CA, 94035

[26] Department of Astrophysical Sciences, Princeton University, 4 Ivy Lane, Princeton, NJ 08544, USA

[27] Tata Institute of Fundamental Research, Mumbai, India

[28] Univ. Paris-Sud, Institut d'Astrophysique Spatiale, UMR 8617, CNRS, Bâtiment 121, 91405 Orsay Cedex, France

[29] Department of Astronomy, Yale University, P.O. Box 208101, New Haven, CT 06520-8101, USA

[30] Max-Planck-Institut fur Sonnensystemforschung, Justus-von-Liebig-Weg 3, 37077 Gottingen, Germany

[31] Center for Space Science, New York University Abu Dhabi, UAE

[32] INAF - Osservatorio Astrofisico di Catania, via S. Sofia 78, 95123, Catania, Italy

[33] Dept. of Chemistry & Physics, Florida Gulf Coast University, 10501 FGCU Blvd. S., Fort Myers, FL 33965 USA

[34] Instituto de Astrofísica e Ciências do Espaço, Universidade do Porto, CAUP, Rua das Estrelas, 4150-762 Porto, Portugal

[35] Departamento de Física e Astronomia, Faculdade de Ciências da Universidade do Porto, Rua do Campo Alegre, s/n, PT4169-007 Porto, Portugal

[36] Department of Astronomy and Space Sciences, Science Faculty, Ege University, 35100, Bornova, İzmir, Turkey

[37] IRAP, Université de Toulouse, CNRS, CNES, UPS, Toulouse, France

[38] Department of Physics, University of Zanjan, Zanjan, Iran

[39] INAF-IAPS, Istituto di Astrofisica e Planetologia Spaziali, Via del Fosso del Cavaliere 100, I-00133 Roma, Italy

[40] IRFU, CEA, Université Paris-Saclay, F-91191 Gif-sur-Yvette, France

[41] AIM, CEA, CNRS, Université Paris-Saclay, Université Paris Diderot, Sorbonne Paris Cité, F-91191 Gif-sur-Yvette, France

[42] Osservatorio Astronomico di Padova – INAF, Vicolo dellOsservatorio 5, I-35122 Padova, Italy

[43] Los Alamos National Laboratory, XTD-NTA, MS T-082, Los Alamos, NM 87545 USA

[44] School of Physics, The University of New South Wales, Sydney NSW 2052, Australia

[45] School of Physics and Astronomy, Sun Yat-Sen University, Guangzhou, 510275, China

[46] Institute of Astrophysics, University of Vienna, 1180 Vienna, Austria

[47] Department of Physics and Astronomy, Iowa State University, Ames, IA 50011 USA

[48] LESIA, CNRS, Université Pierre et Marie Curie, Université Denis, Diderot, Observatoire de Paris, 92195 Meudon cedex, France

[49] Univ Rennes, CNRS, IPR (Institut de Physique de Rennes) - UMR 6251, F-35000 Rennes, France

[50] Zentrum für Astronomie der Universität Heidelberg, Landessternwarte, Königstuhl 12, D-69117 Heidelberg, Germany

[51] Department of Physics and Astronomy, University of North Carolina at Chapel Hill, Chapel Hill, NC 27599, USA

[52] Homi Bhabha Centre for Science Education, TIFR, V. N. Purav Marg, Mankhurd, Mumbai 400088, India

[53] Space Science Institute, 4750 Walnut Street, Suite 205, Boulder CO 80301, USA

[54] Max-Planck-Institut für Sonnensystemforschung, Justus-von-Liebig-Weg 3, 37077, Göttingen, Germany

[55] Astronomy Unit, Queen Mary University of London, Mile End Road, London, E1 4NS, UK

[56] Astrophysics Group, Lennard-Jones Laboratories, Keele University, Staffordshire ST5 5BG, United Kingdom

[57] Vanderbilt University, Department of Physics & Astronomy, 6301 Stevenson Center Ln., Nashville, TN 37235, USA

[58] Vanderbilt Initiative in Data-intensive Astrophysics (VIDA), 6301 Stevenson Center Lane, Nashville, TN 37235, USA

[59] Hubble Fellow

[60] Research School of Astronomy and Astrophysics, Australian National University, Canberra, ACT 2611, Australia

[61] Physics Department, Austin College, Sherman, TX 75090, USA

[62] Caltech/IPAC-NASA Exoplanet Science Institute, Pasadena, CA 91125, USA

[63] Exoplanetary Science at UNSW, School of Physics, UNSW Sydney, NSW 2052, Australia

[64] Department of Physics and Astronomy, George Mason University 4400 University Ave, Fairfax, VA 22030

[65] SGT Inc/NASA Ames Research Center, Moffett Field, CA, 94035

[66] Proto-Logic Consulting LLC, Washington, DC 20009, USA

[67] Université Côte d'Azur, Observatoire de la Côte d'Azur, CNRS, Laboratoire Lagrange, France

[68] Univ. Federal do Rio G. do Norte, UFRN, Dep. de Fsica, CP 1641, 59072-970, Natal, RN, Brazil

[69] Carnegie Institution of Washington DTM, 5241 Broad Branch Road NW, Washington, DC 20015, USA

[70] Section of Astrophysics, Astronomy and Mechanics, Faculty of Physics, National and Kapodistrian University of Athens, GR-15784 Zografos, Athens, Greece

[71] Missouri State University

[72] LinkedIn work performed at NASA Ames Research Center, Moffett Field, CA, 94035

[73] Space Telescope Science Institute, 3700 San Martin Drive, Baltimore, MD 21212

[74] *MTA CSFK, Konkoly Observatory, Budapest, Konkoly Thege Miklós út 15-17, H-1121, Hungary*
[75] *MTA CSFK Lendület Near-Field Cosmology Research Group*
[76] *Mississippi State University, Department of Physics & Astronomy, Hilbun Hall, Starkville, MS, 39762, USA*
[77] *Observatories of the Carnegie Institution for Science, 813 Santa Barbara Street, Pasadena, CA 91101*
[78] *University of Southern Queensland, Toowoomba, Qld 4350, Australia*

ABSTRACT

We present the discovery of TOI-197.01, the first transiting planet identified by the *Transiting Exoplanet Survey Satellite* (*TESS*) for which asteroseismology of the host star is possible. TOI-197 (HIP 116158) is a bright ($V = 8.2$ mag), spectroscopically classified subgiant which oscillates with an average frequency of about $430\,\mu$Hz and displays a clear signature of mixed modes. The oscillation amplitude confirms that the redder *TESS* bandpass compared to *Kepler* has a small effect on the oscillations, supporting the expected yield of thousands of solar-like oscillators with *TESS* 2-minute cadence observations. Asteroseismic modeling yields a robust determination of the host star radius ($R_\star = 2.943 \pm 0.064 R_\odot$), mass ($M_\star = 1.212 \pm 0.074 M_\odot$) and age ($4.9 \pm 1.1$ Gyr), and demonstrates that it has just started ascending the red-giant branch. Combining asteroseismology with transit modeling and radial-velocity observations, we show that the planet is a "hot Saturn" ($R_p = 9.17 \pm 0.33 R_\oplus$) with an orbital period of ~ 14.3 days, irradiance of $F = 343 \pm 24 F_\oplus$, moderate mass ($M_p = 60.5 \pm 5.7 M_\oplus$) and density ($\rho_p = 0.431 \pm 0.062\,$g cm^{-3}). The properties of TOI-197.01 show that the host-star metallicity – planet mass correlation found in sub-Saturns ($4 - 8R_\oplus$) does not extend to larger radii, indicating that planets in the transition between sub-Saturns and Jupiters follow a relatively narrow range of densities. With a density measured to $\sim 15\%$, TOI-197.01 is one of the best characterized Saturn-sized planets to date, augmenting the small number of known transiting planets around evolved stars and demonstrating the power of *TESS* to characterize exoplanets and their host stars using asteroseismology.

Keywords: planets and satellites: individual (TOI-197) — stars: fundamental parameters — techniques: asteroseismology, photometry, spectroscopy — TESS — planetary systems

1. INTRODUCTION

Asteroseismology is one of the major success stories of the space photometry revolution initiated by CoRoT (Baglin et al. 2006) and *Kepler* (Borucki et al. 2010). The detection of oscillations in thousands of stars has led to breakthroughs such as the discovery of rapidly rotating cores in subgiants and red giants, as well as the systematic measurement of stellar masses, radii and ages (see Chaplin & Miglio 2013, for a review). Asteroseismology has also become the "gold standard" for calibrating more indirect methods to determine stellar parameters such as surface gravity ($\log g$) from spectroscopy (Petigura et al. 2017a) and stellar granulation (Mathur et al. 2011; Bastien et al. 2013; Kallinger et al. 2016; Corsaro et al. 2017; Bugnet et al. 2018; Pande et al. 2018), and age from rotation periods (gyrochronology, e.g. García et al. 2014; van Saders et al. 2016).

A remarkable synergy that emerged from space-based photometry is the systematic characterization of exoplanet host stars using asteroseismology. Following first asteroseismic studies of exoplanet host stars using radial velocities (Bouchy et al. 2005; Bazot et al. 2005), the Hubble Space Telescope (Gilliland et al. 2011) and

CoRoT (Ballot et al. 2011b; Lebreton & Goupil 2014), *Kepler* enabled the systematic characterization of exoplanets with over 100 detections of oscillations in host stars to date (Huber et al. 2013a; Lundkvist et al. 2016). In addition to the more precise characterization of exoplanet radii and masses (Ballard et al. 2014), the synergy also enabled systematic constraints on stellar spin-orbit alignments (Chaplin et al. 2014b; Benomar et al. 2014; Lund et al. 2014; Campante et al. 2016a) and statistical inferences on orbital eccentricities through constraints on the mean stellar density (Sliski & Kipping 2014; Van Eylen & Albrecht 2015; Van Eylen et al. 2019).

The recently launched NASA *TESS* Mission (Ricker et al. 2014) is poised to continue the synergy between asteroseismology and exoplanet science. Using dedicated 2-minute cadence observations, *TESS* is expected to detect oscillations in thousands of main-sequence, subgiant and early red-giant stars (Schofield et al. 2018), and simulations predict that at least 100 of these will host transiting or non-transiting exoplanets (Campante et al. 2016b). *TESS* host stars are on average significantly brighter than typical *Kepler* hosts, facilitating ground-based measurements of planet masses with pre-

cisely characterized exoplanet hosts from asteroseismology. While some of the first exoplanets discovered with *TESS* orbit stars that have evolved off the main sequence (Wang et al. 2019; Brahm et al. 2018; Nielsen et al. 2019), none of them were amenable to asteroseismology using *TESS* photometry. Here, we present the characterization of TESS Object of Interest 197 (TOI-197, HIP 116158) system, the first discovery by *TESS* of a transiting exoplanet around a host star in which oscillations can be measured.

2. OBSERVATIONS

2.1. *TESS Photometry*

TESS observed TOI-197 in 2-minute cadence during Sector 2 of Cycle 1 for 27 days. We used the target pixel files produced by the TESS Science Processing Operations Center (Jenkins et al. 2016) as part of the TESS alerts on November 11 2018[1]. We produced a light curve using the photometry pipeline[2] (Handberg et al., in prep.) maintained by the TESS Asteroseismic Science Operations Center (TASOC, Lund et al. 2017), which is based on software originally developed to generate light curves for data collected by the K2 Mission (Lund et al. 2015).

Figure 1a shows the raw light curve obtained from the TASOC pipeline. The coverage is nearly continuous (duty cycle $\sim 93\%$), with a ~ 2 day gap separating the two spacecraft orbits in the observing sector. Two $\sim 0.1\%$ brightness dips, which triggered the identification of TOI-197.01 as a planet candidate, are evident near the beginning of each *TESS* orbit (see upward triangles in Figure 1a). The structure with a period of ~ 2.5 d corresponds to instrumental variations due to the angular momentum dumping cycle of the spacecraft.

To prepare the raw light curve for an asteroseismic analysis, the current TASOC pipeline implements a series of corrections as described by Handberg & Lund (2014), which includes removal of instrumental artefacts and of the transit events using a combination of filters utilizing the estimated planetary period. Future TASOC-prepared light curves from full *TESS* data releases will use information from the ensemble of stars to remove common instrumental systematics (Lund et al, in prep.). Alternative light curve corrections using transit removal and gap interpolation (García et al. 2011; Pires et al. 2015) yielded consistent results. The corrected TASOC light curve is shown in Figure 1b. Figure 1c shows a power spectrum of this light curve, revealing

the clear presence of a granulation background and a power excess from solar-like oscillations near $\sim 430\,\mu$Hz, both characteristic of an evolved star near the base of the red-giant branch.

2.2. *High-Resolution Spectroscopy*

We obtained high-resolution spectra of TOI-197 using several facilities within the TESS Follow-up Observation Program (TFOP), including HIRES (Vogt et al. 1994) on the 10-m telescope at Keck Observatory (Maunakea, Hawai'i), the Hertzsprung SONG Telescope at Teide Observatory (Tenerife) (Grundahl et al. 2017), HARPS (Mayor et al. 2003), FEROS (Kaufer et al. 1999), Coralie (Queloz et al. 2001) and FIDEOS (Vanzi et al. 2018) on the MPG/ESO 3.6-m, 2.2-m, 1.2-m, and 1-m telescopes at La Silla Observatory (Chile), Veloce (Gilbert et al. 2018) on the 3.9-m Anglo-Australian Telescope at Siding Spring Observatory (Australia), TRES (Fürész 2008) on the 1.5-m Tillinghast reflector at the F. L. Whipple Observatory (Mt. Hopkins, Arizona), and iSHELL (Rayner et al. 2012) on the NASA IRTF Telescope (Maunakea, Hawaii). All spectra used in this paper were obtained between Nov 11 and Dec 30 2018 and have a minimum spectral resolution of $R \approx 44000$. FEROS, Coralie, and HARPS data were processed and analyzed with the CERES package (Brahm et al. 2017a), which performs the optimal extraction and wavelength calibration of each spectrum, along with the measurement of precision radial velocities and bisector spans via the cross-correlation technique. Most instruments have been previously used to obtain precise radial velocities to confirm exoplanets, and we refer to the publications listed above for details on the reduction methods.

To obtain stellar parameters, we analyzed a HIRES spectrum using Specmatch (Petigura 2015), which has been extensively applied for the classification of *Kepler* exoplanet host stars (Johnson et al. 2017; Petigura et al. 2017a). The resulting parameters were $T_{\rm eff} = 5080 \pm 70$ K, $\log g = 3.60 \pm 0.08$ dex, [Fe/H] $= -0.08 \pm 0.05$ dex and $v \sin i = 2.8 \pm 1.6$ km s^{-1}, consistent with an evolved star as identified from the power spectrum in Figure 1c. To account for systematic differences between spectroscopic methods (Torres et al. 2012) we added 59 K in $T_{\rm eff}$ and 0.062 dex in [Fe/H] in quadrature to the formal uncertainties, yielding final values of $T_{\rm eff} = 5080 \pm 90$ K and [Fe/H] $= -0.08 \pm 0.08$ dex. Independent spectroscopic analyses yielded consistent results, including an analysis of a HIRES spectrum using ARES+MOOG (Sousa 2014; Sousa et al. 2018), FEROS spectra using ZASPE (Brahm et al. 2017b), TRES spectra using SPC (Buchhave et al. 2012) and iSHELL spectra using BT-Settl models (Allard et al. 2012).

---

[1] https://doi.org/10.17909/t9-wx1n-aw08
[2] https://tasoc.dk/code/
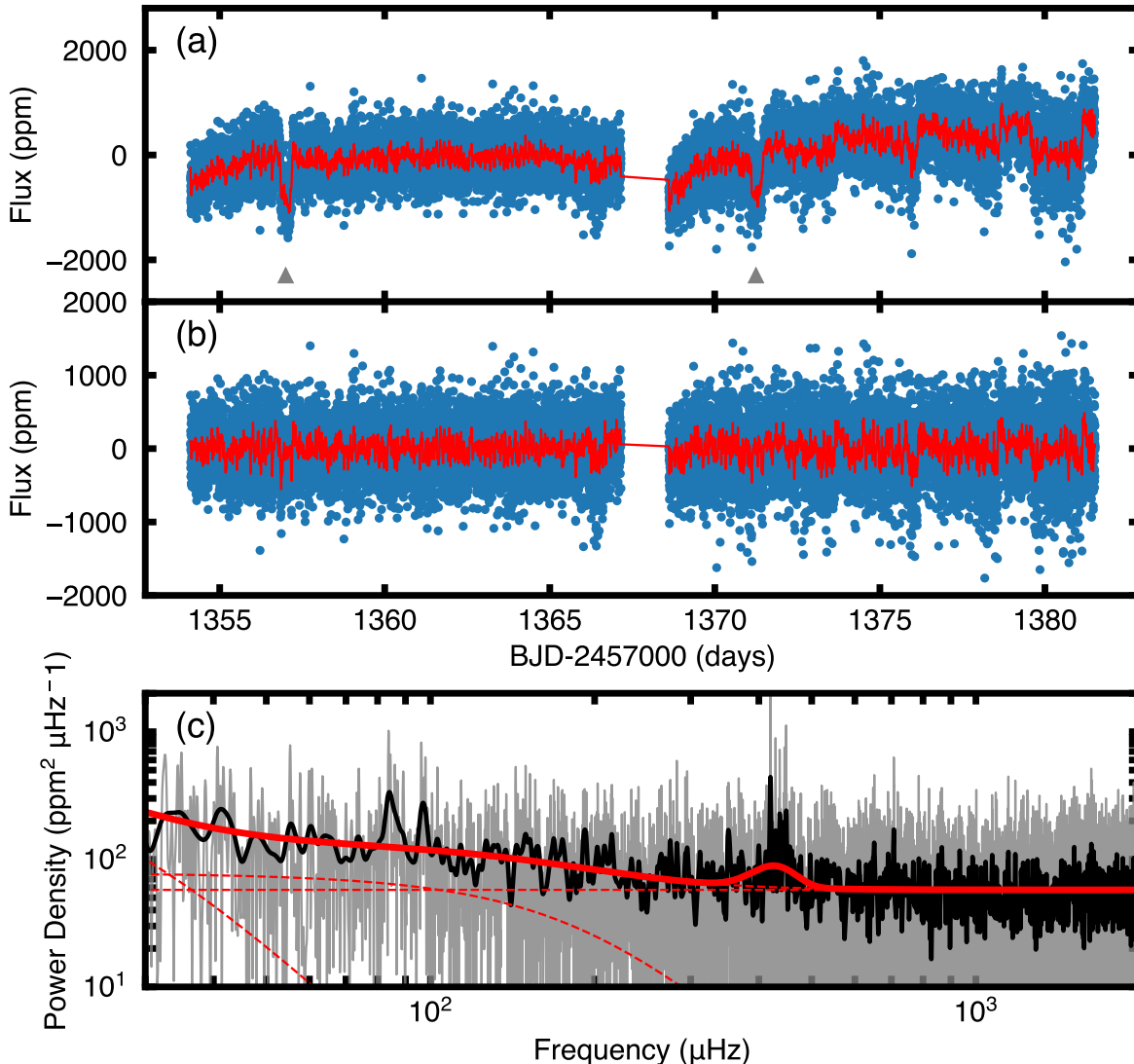
Figure 1. Panel (a): Raw *TESS* 2-minute cadence light curve of TOI-197 produced by the TESS Asteroseismic Science Operations Center (TASOC). The red line is the light curve smoothed with a 10-minute boxcar filter (shown for illustration purposes only). Upward triangles mark the two transit events. Panel (b): Light curve after applying corrections by the TASOC pipeline. Panel (c): Power spectrum of panel (b), showing a granulation background and power excess due to oscillations near $\sim 430\,\mu$Hz. The solid red line is a global fit, consisting of granulation plus white noise and a Gaussian describing the power excess due to oscillations. Dashed red lines show the two granulation components and the white noise level, respectively.

2.3. *Broadband Photometry & Gaia Parallax*

We fitted the spectral energy distribution (SED) of TOI-197 using broadband photometry following the method described by Stassun & Torres (2016). We used NUV photometry from *GALEX*, $B_T V_T$ from *Tycho-2* (Høg et al. 2000), $BVgri$ from APASS, JHK_S from *2MASS* (Skrutskie et al. 2006), W1–W4 from *WISE* (Wright et al. 2010), and the G magnitude from *Gaia* (Evans et al. 2018). The data were fit using Kurucz atmosphere models, with $T_{\rm eff}$, [Fe/H] and extinction (A_V) as free parameters. We restricted A_V to

the maximum line-of-sight value from the dust maps of Schlegel et al. (1998). The resulting fit yielded $T_{\rm eff} = 5090 \pm 85$ K, [Fe/H] $= -0.3 \pm 0.3$ dex, and $A_V = 0.09 \pm 0.02$ mag with reduced χ^2 of 1.9, in good agreement with spectroscopy. Integrating the (dereddened) model SED gives the bolometric flux at Earth of $F_{\rm bol} = 1.88 \pm 0.04 \times 10^{-8}$ erg s cm^{-2}. An independent SED fit using 2MASS, APASS9, USNO-B1 and WISE photometry and Kurucz models yielded excellent agreement, with $F_{\rm bol} = 1.83 \pm 0.09 \times 10^{-8}$ erg s cm^{-2} and $T_{\rm eff} = 5150 \pm 130$ K. Additional independent analyses

using the method by Mann et al. (2016) and PARAM (Rodrigues et al. 2014, 2017) yielded bolometric fluxes and extinction values that are consistent within $1\,\sigma$ with the values quoted above.

Combining the bolometric flux with the *Gaia* DR2 distance allows us to derive a nearly model-independent luminosity, which is a valuable constraint for asteroseismic modeling (see Section 3.3). Using a *Gaia* parallax of 10.518 ± 0.080 mas (adjusted for the 0.082 ± 0.033 mas zero-point offset for nearby stars reported by Stassun & Torres 2018) with the two methods described above yielded $L_\star = 5.30 \pm 0.14 L_\odot$ (using $F_{\rm bol} = 1.88 \pm 0.04 \times 10^{-8}$ erg s cm^{-2}) and $L_\star = 5.13 \pm 0.13 L_\odot$ (using $F_{\rm bol} = 1.83 \pm 0.09 \times 10^{-8}$ erg s cm^{-2}). We also derived a luminosity using `isoclassify` (Huber et al. 2017)[3], adopting 2MASS K-band photometry, bolometric corrections from MIST isochrones (Choi et al. 2016) and the composite reddening map `mwdust` (Bovy et al. 2016), yielding $L_\star = 5.03 \pm 0.13 L_\odot$. Our adopted luminosity was the mean of these methods with an uncertainty calculated by adding the mean uncertainty and scatter over all methods in quadrature, yielding $L_\star = 5.15 \pm 0.17 L_\odot$.

2.4. *High-Resolution Imaging*

TOI-197 was observed with the NIRC2 camera and Altair adaptive optics system on Keck-2 (Wizinowich et al. 2000) on UT 25 November 2018. Conditions were clear but seeing was poor (0.8–2"). We used the science target as the natural guide star and images were obtained through a K-continuum plus KP50$_{1.5}$ filter using the narrow camera (10 mas pixel scale). We obtained eight images (four each at two dither positions), each consisting of 50 co-adds of 0.2 sec each, with correlated double-sampling mode and four reads. Frames were co-added and we subtracted an average dark image, constructed from a set of darks with the same integration time and sampling mode. Flat-fielding was performed using a dome flat obtained in the K' filter. "Hot" pixels were identified in the dark image and corrected by median filtering with a 5×5 box centered on each affected pixel in the science image. Only a single star appears in the images. We performed tests in which "clones" of the stellar image reduced by a specified contrast ratio were added to the original image. These show that we would have been able to detect companions as faint as $\Delta K = 5.8$ mag within 0.4" of TOI-197, 3.8 mag within 0.2", and 1.8 mag within 0.1".

Additional NIRC2 observations were obtained in the narrow-band $Br-\gamma$ filter ($\lambda_o = 2.1686; \Delta\lambda = 0.0326\mu$m) on UT 22 November 2018. A standard 3-point dither

pattern with a step size of $3''$ was repeated twice with each dither offset from the previous dither by $0.5''$. An integration time of 0.25 seconds was used with one coadd per frame for a total of 2.25 seconds on target, and the camera was used in the narrow-angle mode. No additional stellar companions were detected to within a resolution of $\sim 0.05''$ FWHM. The sensitivities of the final combined AO image were determined following Ciardi et al. (2015) and Furlan et al. (2017), with detection limits as faint as $\Delta Br - \gamma = 7.4$ mag within 0.4", 6.1 mag within 0.2", and 3.2 mag within 0.1".

The results from NIRC2 are consistent with Speckle observations using HRCam (Tokovinin et al. 2010) on the 4.1 m SOAR telescope[4]. Since the companion is unlikely to be bluer than TOI-197, these constraints exclude any significant dilution (both for oscillation amplitudes and the depth of transit events).

3. ASTEROSEISMOLOGY

3.1. *Global Oscillation Parameters*

To extract oscillation parameters characterizing the average properties of the power spectrum, we used several automated analysis methods (e.g. Huber et al. 2009; Mathur et al. 2010; Mosser et al. 2012a; Benomar et al. 2012; Kallinger et al. 2012; Corsaro & De Ridder 2014; Lundkvist 2015; Stello et al. 2017; Campante 2018; Bell et al. 2019), many of which have been extensively tested on *Kepler* data (e.g. Hekker et al. 2011; Verner et al. 2011). In most of these analyses, the power contributions due to granulation noise and stellar activity were modeled by a combination of power laws and a flat contribution due to shot noise, and then corrected by dividing the power spectrum by the background model. The individual contributions and background model using the method by Huber et al. (2009) are shown as dashed and solid red lines in Fig. 1c, and a close-up of the power excess is shown in Fig. 2a.

Next, the frequency of maximum power ($\nu_{\rm max}$) was measured either by heavily smoothing the power spectrum or by fitting a Gaussian function to the power excess. Our analysis yielded $\nu_{\rm max} = 430 \pm 18\,\mu$Hz, with uncertainties calculated from the scatter between all fitting techniques. Finally, the mean oscillation amplitude per radial mode was determined by taking the peak of the smoothed, background-corrected oscillation envelope and correcting for the contribution of non-radial modes (Kjeldsen et al. 2008b), yielding $A = 18.7 \pm 3.5$ ppm. We caution that the $\nu_{\rm max}$ and
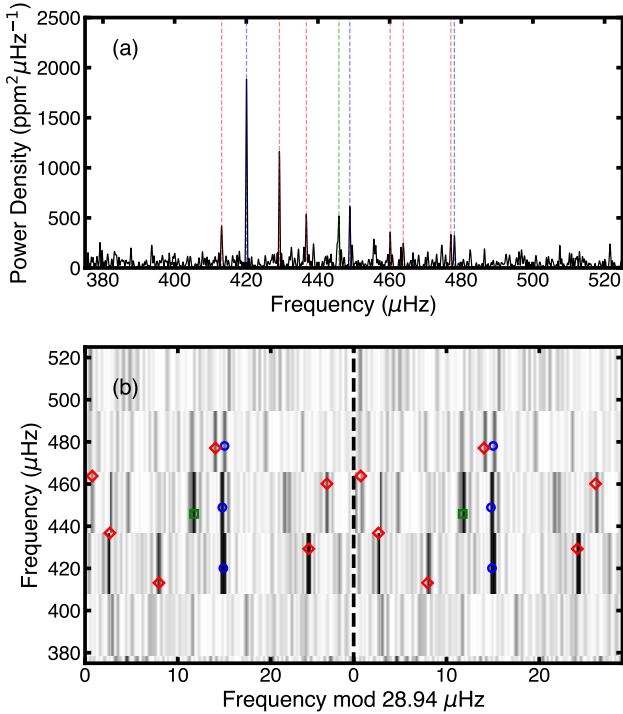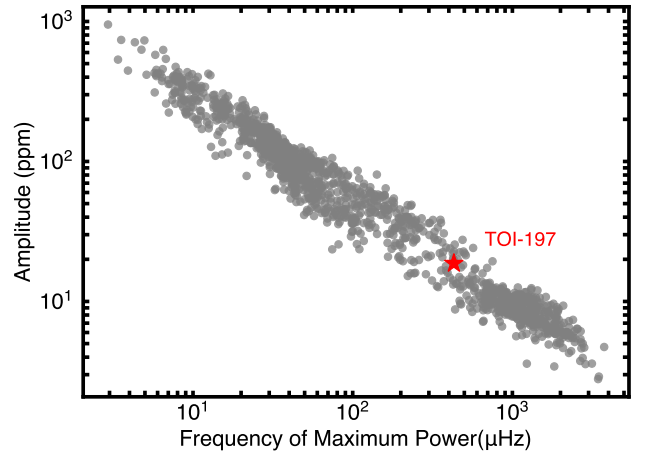

Figure 2. Panel (a): Power spectrum of TOI-197 centered on the frequency region showing oscillations. Vertical dashed lines mark identified individual frequencies. Panel (b): Greyscale échelle diagram[5] of the background-corrected and smoothed power spectrum in panel (a). Identified individual mode frequencies are marked with blue circles ($l = 0$, radial modes), green squares ($l = 2$, quadrupole modes) and red diamonds ($l = 1$, dipole modes). Note that the diagram is replicated for clarity (Bedding 2012).

amplitude estimates could be significantly biased by the stochastic nature of the oscillations. The modes are not well resolved, as demonstrated by the non-Gaussian appearance of the power spectrum and the particularly strong peak at 420 μHz.

Global seismic parameters such as ν_{max} and amplitude follow well-known scaling relations (Huber et al. 2011; Mosser et al. 2012b; Corsaro et al. 2013), which allow us to test whether the detected oscillations are consistent with expectations. Figure 3 compares our measured ν_{max} and amplitude with results for ~1500 stars observed by *Kepler* (Huber et al. 2011). We observe excellent agreement, confirming that the detected

Figure 3. Amplitude per radial mode versus frequency of maximum power for a sample of ~1500 stars spanning from the main-sequence to the red giant branch observed by *Kepler* (Huber et al. 2011). The red star shows the measured position of TOI-197. The uncertainties are approximately equal to the symbol size.

signal is consistent with solar-like oscillations. We note that the oscillations in the *TESS* bandpass are expected to be ~15 % smaller than in the bluer *Kepler* bandpass, which is well within the spread of amplitudes at a given ν_{max} observed in the *Kepler* sample. The result confirms that the redder bandpass of *TESS* only has a small effect on the oscillation amplitude, supporting the expected rich yield of solar-like oscillators with *TESS* 2-minute cadence observations (Schofield et al. 2018).

3.2. *Individual Mode Frequencies*

The power spectrum in Fig. 2a shows several clear peaks corresponding to individual oscillation modes. Given that *TESS* instrument artifacts are not yet well understood, we restricted our analysis to the frequency range 400–500 μHz where we observe peaks well above the background level.

To extract these individual mode frequencies, we used several independent methods ranging from traditional iterative sine-wave fitting, i.e., pre-whitening (e.g. Lenz & Breger 2005; Kjeldsen et al. 2005; Bedding et al. 2007), to fitting of Lorentzian mode profiles (e.g. Handberg & Campante 2011; Appourchaux et al. 2012; Mosser et al. 2012b; Corsaro & De Ridder 2014; Corsaro et al. 2015; Vrard et al. 2015; Davies & Miglio 2016; Roxburgh 2017; Handberg et al. 2017; Kallinger et al. 2018), including publicly available code such as DIAMONDS[6]. We required at least two independent meth-

---

[5] Échelle diagrams are constructed by dividing a power spectrum into equal segments with length $\Delta\nu$ and stacking one above the other, so that modes with a given spherical degree align vertically in ridges (Grec et al. 1983). Departures from regularity arise from sound speed discontinuities and from mixed modes, and thus probe the interior structure of a star.

[6] https://github.com/EnricoCorsaro/DIAMONDS

Table 1. Extracted oscillation frequencies and mode identifications for TOI-197.

$f(\mu Hz)$	$\sigma_f(\mu Hz)$	l
413.12	0.29	1
420.06	0.11	0
429.26	0.14	1
436.77	0.24	1
445.85	0.21	2
448.89	0.21	0
460.16	0.33	1
463.81	0.43	1
477.08	0.31	1
478.07	0.35	0

Note: The large frequency separation derived from radial modes is $\Delta\nu = 28.94 \pm 0.15\mu Hz$. Note that the $l = 1$ modes at ~ 460 and $\sim 463\,\mu Hz$ are listed for completeness, but it is unlikely that both of them are genuine (see text).

ods to return the same frequency within uncertainties and that the posterior probability of each peak being a mode was $\geq 90\%$ (Basu & Chaplin 2017). A comparison of the frequencies returned by different fitters showed very good agreement, at a level smaller than the uncertainties for all the reported modes. For the final list of frequencies we adopted values from one fitter who applied pre-whitening (HK), with uncertainties derived from Monte Carlo simulations of the data, as listed in Table 1.

To measure the large frequency separation $\Delta\nu$, we performed a linear fit to all identified radial modes, yielding $\Delta\nu = 28.94 \pm 0.15\mu Hz$. Figure 2b shows a greyscale échelle diagram[5] using this $\Delta\nu$ measurement, including the extracted mode frequencies. The $l = 1$ modes are strongly affected by mode bumping, as expected for the mixed mode coupling factors for evolved stars in this evolutionary stage. The offset ϵ of the $l = 0$ ridge is ~ 1.5, consistent with the expected value from *Kepler* measurements for stars with similar $\Delta\nu$ and $T_{\rm eff}$ (White et al. 2011).

3.3. *Frequency Modeling*

We used a number of independent approaches to model the observed oscillation frequencies, including different stellar evolution codes (ASTEC, Cesam2K, GARSTEC, Iben, MESA, and YREC, Christensen-Dalsgaard 2008; Morel & Lebreton 2008; Scuflaire et al. 2008; Weiss et al. 2008; Iben 1965; Paxton et al. 2011, 2013, 2015; Choi et al. 2016; Demarque et al. 2008), oscillation codes (ADIPLS, GYRE and Pesnell, Christensen-Dalsgaard 2008; Townsend & Teitler 2013; Pesnell 1990) and modeling methods (including AMP,
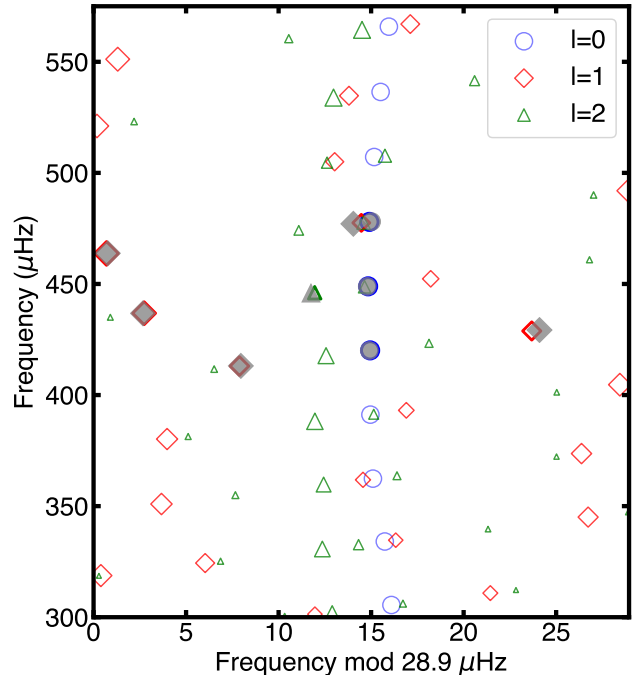
Figure 4. Échelle diagram showing observed oscillation frequencies (filled grey symbols) and a representative best-fitting model (open colored symbols) using GARSTEC, ADIPLS and BeSSP (Serenelli et al. 2017). Model symbol sizes for non-radial modes are scaled using the mode inertia (a proxy for mode amplitude) as described in Cunha et al. (2015). Thick model symbols correspond to modes that were matched to observations. Uncertainties on the observed frequencies are than smaller or comparable to the symbol sizes. Note that the $l = 1$ mode at $460\,\mu Hz$ has been omitted from this plot (see text).

ASTFIT, BeSSP, BASTA, PARAM, Creevey et al. 2017; Silva Aguirre et al. 2015; Serenelli et al. 2017; Rodrigues et al. 2014, 2017; Deheuvels & Michel 2011; Yıldız et al. 2016; Ong & Basu 2019; Tayar & Pinsonneault 2018; Lebreton & Goupil 2014; Ball & Gizon 2017; Mosumgaard et al. 2018). Most of the adopted methods applied corrections for the surface effect (Kjeldsen et al. 2008a; Ball & Gizon 2017). Model inputs included the spectroscopic temperature and metallicity, individual frequencies, $\Delta\nu$, and the luminosity (Section 2.3). To investigate the effects of different input parameters, modelers were asked to provide solutions using both individual frequencies and only using $\Delta\nu$, with and without taking into account the luminosity constraint. The constraint on $\nu_{\rm max}$ was not used in the modeling since it may be affected by finite mode lifetimes (see Section 3.1).

Overall, the modeling efforts yielded consistent results, and most modeling codes were able to provide adequate fits to the observed oscillation frequencies. The

Basic Properties

Hipparcos ID	116158
TIC ID	441462736
V Magnitude	8.15
TESS Magnitude	7.30
K Magnitude	6.04

SED & *Gaia* Parallax

Parallax, π (mas)	10.518 ± 0.080
Luminosity, L ($L_\odot$)	5.15 ± 0.17

Spectroscopy

Effective Temperature, $T_{\rm eff}$ (K)	5080 ± 90
Metallicity, [Fe/H] (dex)	-0.08 ± 0.08
Projected rotation speed, $v \sin i$ (km s^{-1})	2.8 ± 1.6

Asteroseismology

Stellar Mass, $M_\star$ ($M_\odot$)	1.212 ± 0.074
Stellar Radius, $R_\star$ ($R_\odot$)	2.943 ± 0.064
Stellar Density, $\rho_\star$ (gcc)	0.06702 ± 0.00067
Surface gravity, $\log g$ (cgs)	3.584 ± 0.010
Age, t (Gyr)	4.9 ± 1.1

Notes: The *TESS* magnitude is adopted from the TESS Input Catalog (Stassun et al. 2018).

modeling confirmed that only one of the two closely-spaced mixed modes near $\sim 460\,\mu$Hz is likely real, but we have retained both frequencies in Table 1 for consistency. An échelle diagram with observed frequencies and a representative best-fitting model is shown in Figure 4.

Independent analyses confirmed a bimodality splitting into lower-mass, older models ($\sim 1.15 M_\odot$, ~ 6 Gyr) and higher-mass, younger models ($\sim 1.3 M_\odot$, ~ 4 Gyr). Surface rotation would provide an independent mass diagnostic (e.g. van Saders & Pinsonneault 2013), but the insufficiently constrained $v \sin i$ and the unknown stellar inclination mean that we cannot decisively break this degeneracy. Combining an independent constraint of $\log g = 3.603 \pm 0.026$ dex from an autocorrelation analysis of the light curve (Kallinger et al. 2016) with a radius from L and $T_{\rm eff}$ favors a higher-mass solution ($M_\star = 1.27 \pm 0.13 M_\odot$), but may be prone to small systematics in the $\nu_{\rm max}$ scaling relation (which was used for the calibration). To make use of the most observational constraints available, we used the set of nine modeling solutions which used $T_{\rm eff}$, [Fe/H], frequencies and the luminosity as input parameters. From this set of solutions, we adopted the self-consistent set of stellar

Time (BJD)	RV (m/s)	$\sigma_{\rm RV}$ (m/s)	Instrument
2458426.334584	4.258	11.260	SONG
2458426.503655	6.328	11.270	SONG
2458427.575230	-12.667	3.000	FEROS
2458428.547576	17.328	18.540	SONG
...	...	...	...
2458443.535340	-14.667	3.600	CORALIE
2458443.541210	-3.067	3.800	CORALIE
2458443.714865	-6.815	0.780	HIRES
2458443.825283	-4.375	0.720	HIRES
...	...	...	...
2458482.562290	19.433	2.000	HARPS
2458483.541710	16.133	2.000	HARPS
2458483.553240	19.233	2.000	HARPS
2458483.564690	16.233	2.000	HARPS

Notes: Error bars do not include contributions from stellar jitter and measurements have not been corrected for zeropoint offsets. This table is available in its entirety in a machine-readable form in the online journal.

parameters with the mass closest to the median mass over all results. A more detailed study of the individual modeling results will be presented in a follow-up paper (Li et al., in prep).

For ease of propagating stellar parameters to exoplanet modeling (see next section), uncertainties were calculated by adding the median uncertainty for a given stellar parameter in quadrature to the standard deviation of the parameter for all methods. This method has been commonly adopted for *Kepler* (e.g. Chaplin et al. 2014a) and captures both random and systematic errors estimated from the spread among different methods. For completeness, the individual random and systematic error estimates are $R_\star = 2.943 \pm 0.041({\rm ran}) \pm 0.049({\rm sys})\,{\rm R}_\odot$, $M_\star = 1.212 \pm 0.052({\rm ran}) \pm 0.055({\rm sys})\,{\rm M}_\odot$, $\rho_\star = 0.06702 \pm 0.00019({\rm ran}) \pm 0.00047({\rm sys})\,{\rm gcc}$, and $t = 4.9 \pm 0.6({\rm ran}) \pm 0.9({\rm sys})\,{\rm Gyr}$. This demonstrates that systematic errors constitute a significant fraction of the error budget for all stellar properties (in particular stellar age), and emphasize the need for using multiple model grids to derive realistic uncertainties for stars and exoplanets. The final estimates of stellar parameters are summarized in Table 2, constraining the radius, mass, density and age of TOI-197 to $\sim 2\,\%$, $\sim 6\,\%$, $\sim 1\,\%$ and $\sim 22\,\%$.

4. PLANET CHARACTERIZATION

To fit the transits observed in the *TESS* data we used the PDC-MAP light curve provided by the TESS Science Processing and Operations Center (SPOC), which
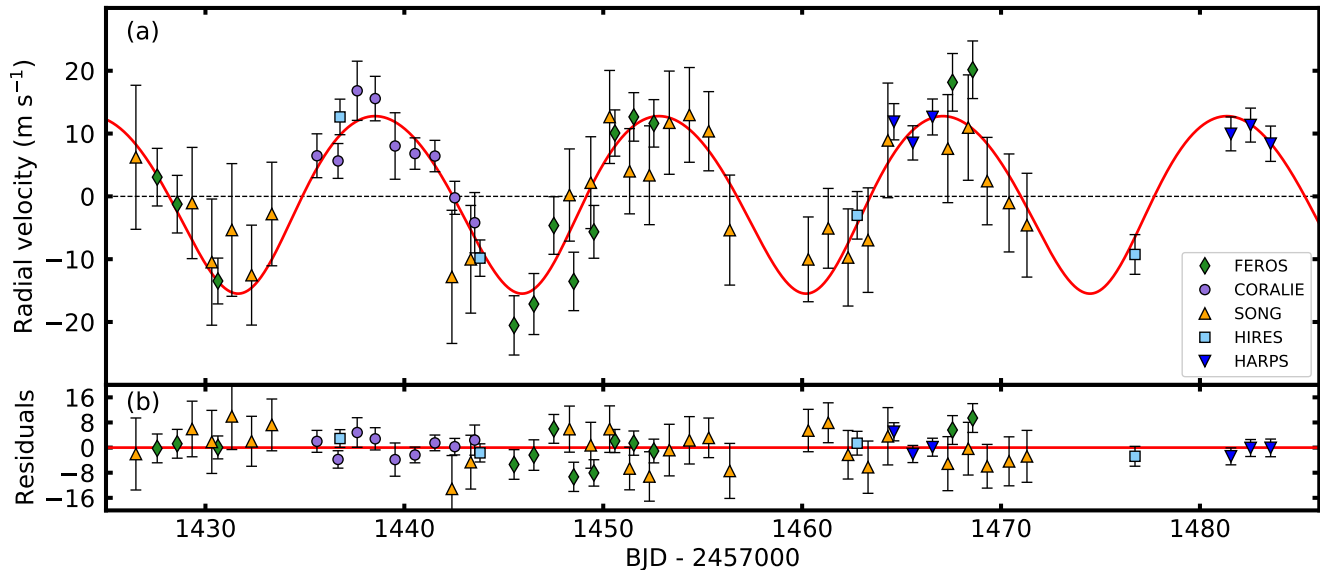
Figure 5. Radial velocity timeseries (panel a) and residuals after subtracting the best-fitting model (panel b) for TOI-197. Datapoints are corrected for zeropoint offsets of individual instruments, and error bars include contributions from stellar jitter.

has been optimized to remove instrumental variability and preserve transits (Smith et al. 2012; Stumpe et al. 2014). To optimize computation time we discarded all data more than 2.5 days before and after each of the two observed transits. We have repeated the fit and data preparation procedure using the TASOC light curve and found consistent results.

A total of 107 radial velocity measurements from five different instruments (see Section 2.2 and Table 3) were used to constrain the mass of the planet. No spectroscopic observations were taken during transits, and hence the measurements are unaffected by the Rossiter-McLaughlin effect ($\sim 2.3\,\mathrm{m\,s^{-1}}$ based on the measured $v \sin i$ and $R_p/R_\star$). To remove variations from stellar oscillations, we calculated weighted nightly means for all instruments which obtained multiple observations per night. We performed a joint transit and radial-velocity fit using a Markov Chain Monte Carlo algorithm based on the exoplanet modeling code `ktransit` (Barclay 2018), as described in Chontos et al. (2019). We placed a strong Gaussian prior on the mean stellar density using the value derived from asteroseismology (Table 2) and weak priors on the linear and quadratic limb darkening coefficients, derived from the closest I-band grid points in Claret & Bloemen (2011), with a width of 0.6 for both coefficients. We also adopted a prior for the radial-velocity jitter from granulation and oscillations of $2.5 \pm 1.5\,\mathrm{m\,s^{-1}}$, following Yu et al. (2018) (see also Tayar et al. 2018), and a $1/e$ prior on the eccentricity to account for the linear bias introduced by sampling in $e \cos \omega$ and $e \sin \omega$ (Eastman et al. 2013). Independent

zeropoint offsets and stellar jitter values for each of the five instruments that provided radial velocities. Independent joint fits using EXOFASTv2 (Eastman et al. 2013) yielded consistent results.

Figures 5 and 6 show the radial velocity timeseries, phase-folded transit and RV data, and the corresponding best-fitting model. Table 4 lists the summary statistics for all planet and model parameters. The system is well described by a planet in a 14.3 day orbit, which is nearly equal in size but $\sim 35\%$ less massive than Saturn ($R_\mathrm{p} = 0.836 \pm 0.031\,R_\mathrm{J}$, $M_\mathrm{p} = 0.190 \pm 0.018\,M_\mathrm{J}$), with tentative evidence for a mild eccentricity ($e = 0.11 \pm 0.03$). The long transit duration (~ 0.5 days) is consistent with a non-grazing ($b \approx 0.7$) transit given the asteroseismic mean stellar density, providing further confirmation for a gas-giant planet orbiting an evolved star. The radial velocity data do not show evidence for any other short-period companions. Continued monitoring past the ~ 4 orbital periods covered here will further reveal details about the orbital architecture of this system.

5. DISCUSSION

TOI-197.01 joins an enigmatic but growing class of transiting planets orbiting stars that have significantly evolved off the main sequence. Figure 7 compares the position of TOI-197 within the expected population of solar-like oscillators to be detected with *TESS* (panel a) and within the known population of exoplanet host stars. Evolutionary states in Figure 7b have been assigned using solar-metallicity PARSEC evolutionary tracks (Bressan et al. 2012) as described in Berger et al.

Table 4. Planet Parameters

Parameter	Best-fit	Median	84%	16%
Model Parameters				
γ_{HIRES}	4.8	5.4	+1.6	−1.6
γ_{SONG}	1.1	0.2	+1.5	−1.5
γ_{FEROS}	-15.4	-15.7	+1.2	−1.2
$\gamma_{\mathrm{CORALIE}}$	-5.4	-5.0	+1.2	−1.2
γ_{HARPS}	8.1	8.8	+1.5	−1.5
σ_{HIRES}	2.71	2.68	+0.85	−0.80
σ_{SONG}	2.06	2.11	+0.91	−0.89
σ_{FEROS}	3.49	3.47	+0.75	−0.71
$\sigma_{\mathrm{CORALIE}}$	1.88	2.50	+0.75	−0.64
σ_{HARPS}	2.41	2.69	+0.75	−0.63
z (ppm)	199.4	199.1	+10.6	−10.7
P (days)	14.2762	14.2767	+0.0037	−0.0037
T_0 (BTJD)	1357.0135	1357.0149	+0.0025	−0.0026
b	0.744	0.728	+0.040	−0.049
$R_p/R_\star$	0.02846	0.02854	+0.00084	−0.00071
$e\cos\omega$	-0.054	-0.028	+0.063	−0.061
$e\sin\omega$	-0.099	-0.096	+0.029	−0.030
K (m/s)	14.6	14.1	+1.2	−1.2
$\rho_\star(\rho_\odot)$	0.06674	0.06702	+0.00052	−0.00052
u1	0.12	0.35	+0.36	−0.24
u2	0.71	0.44	+0.30	−0.44
Derived Properties				
e	0.113	0.115	+0.034	−0.030
ω	-118.7	-106.0	+34.7	−31.1
a (AU)	0.1233	0.1228	+0.0025	−0.0026
$a/R_\star$	9.00	8.97	+0.27	−0.27
i (°)	85.67	85.75	+0.36	−0.35
$R_{\mathrm{p}}(R_\oplus)$	9.16	9.17	+0.34	−0.31
$R_{\mathrm{p}}(R_{\mathrm{J}})$	0.835	0.836	+0.031	−0.028
$M_{\mathrm{p}}(M_\oplus)$	63.4	60.5	+5.7	−5.7
$M_{\mathrm{p}}(M_{\mathrm{J}})$	0.200	0.190	+0.018	−0.018
ρ_{p} (gcc)	0.455	0.431	+0.064	−0.060

Notes: Parameters denote velocity zeropoints γ, radial velocity jitter σ, photometric zero point z, orbital period P, time of transit T_0, impact parameter b, star-to-planet radius ratio $R_p/R_\star$, eccentricity e, argument of periastron ω, radial velocity semi-amplitude K, mean stellar density $\rho_\star$, linear and quadratic limb darkening coefficients u_1 and u_2, semi-major axis a, orbital inclination i, as well as planet radius (R_{p}), mass (M_{p}) and density (ρ_{p}).
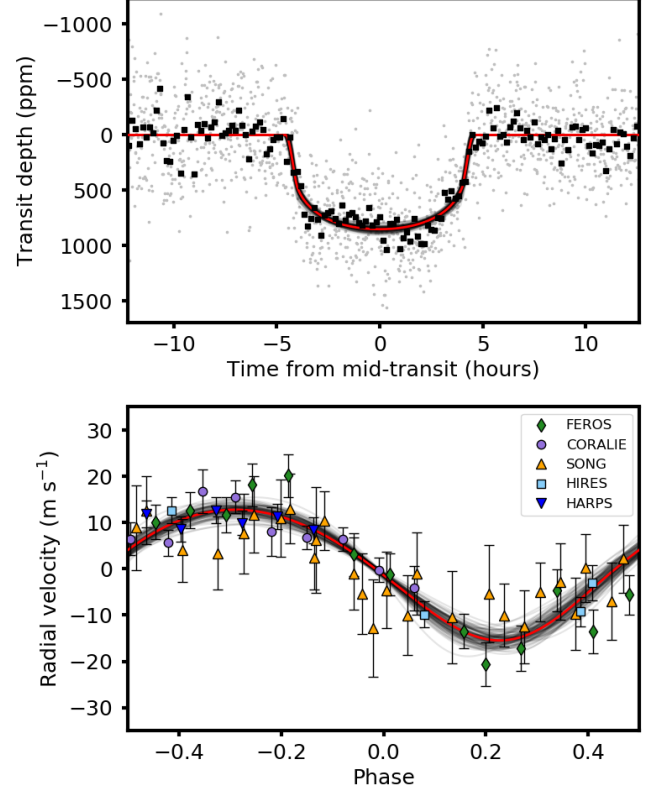
Figure 6. *TESS* light curve (panel a) and radial-velocity measurements (panel b) folded with the best fitting orbital period. Grey points in panel a show the original sampling, and black points are binned means over 10 minutes. Red lines in both pabels show the best-fitting model from the joint fit using stellar parameters, transit and radial velocities. Grey lines show random draws from the joint MCMC model. Error bars in panel b include contributions from stellar jitter.

(2018)[6]. TOI-197 sits at the boundary between subgiants and red giants, with the measured $\Delta\nu$ value indicating that the star has just started its ascent on the red-giant branch (Mosser et al. 2014). TOI-197 is a typical target for which we expect to detect solar-like oscillations with *TESS*, predominantly due to the increased oscillation amplitude, which are well known to scale with luminosity (Kjeldsen & Bedding 1995). On the contrary, TOI-197 is rare among known exoplanet hosts: while radial velocity searches have uncovered a large number of planets orbiting red giants on long orbital periods (e.g. Wittenmyer et al. 2011), less than 15 transiting planets are known around red-giant stars (as defined in Figure 7b). TOI-197 is the sixth example of a transiting planet orbiting a late subgiant / early red giant with detected oscillations, following Kepler-91

---

[6]see also https://github.com/danxhuber/evolstate
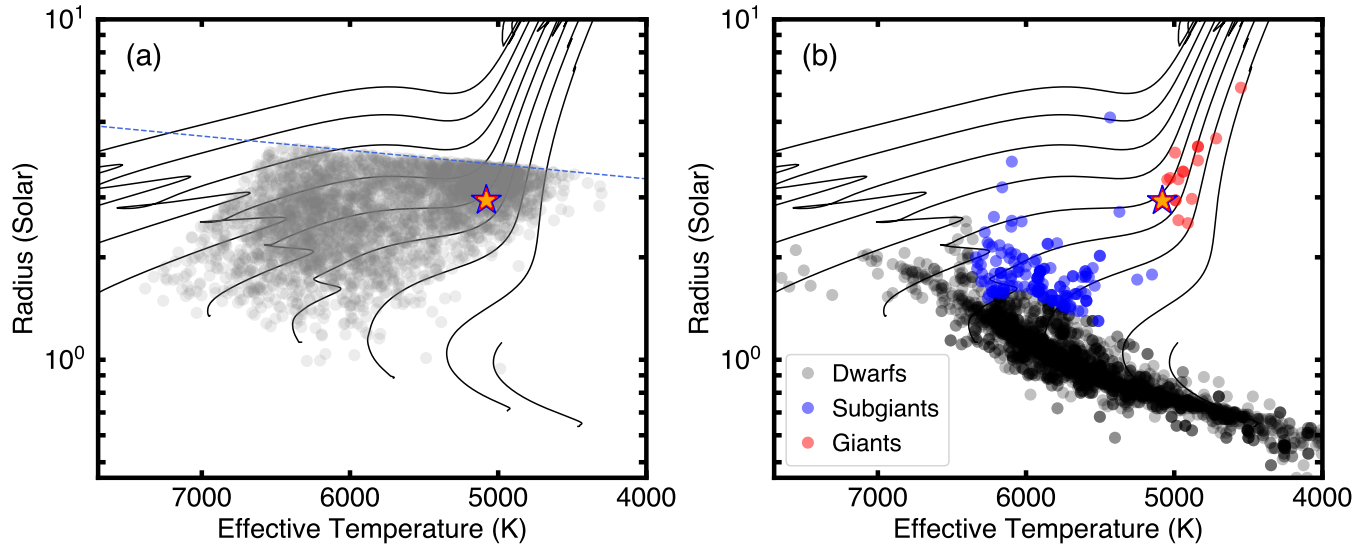
Figure 7. Stellar radius versus effective temperature for the expected *TESS* Cycle 1 yield of solar-like oscillators (panel a, Schofield et al. 2018) and for all stars with confirmed transiting planets (panel b). The blue dashed line in panel a marks the approximate limit below which 2-minute cadence data is required to sample the oscillations. Symbols in panel b are color-coded according to the evolutionary state of the star using solar-metallicity PARSEC evolutionary tracks. TOI-197 falls on the border between subgiants and red-giants, and is highlighted with an orange/red/blue star symbol. TOI-197 is a typical target for which we expect to detect solar-like oscillations with *TESS*, but occupies a rare parameter space for an exoplanet host.

(Barclay et al. 2013), Kepler-56 (Steffen et al. 2012; Huber et al. 2013b), Kepler-432 (Quinn et al. 2015), K2-97 (Grunblatt et al. 2016) and K2-132 (Grunblatt et al. 2017; Jones et al. 2018).

Transiting planets orbiting evolved stars are excellent systems to advance our understanding of the effects of stellar evolution on the structure and evolution of planets (see e.g. Veras 2016, for a review). For example, such systems provide the possibility to test the effects of stellar mass, evolution and binarity on planet occurrence (e.g. Johnson et al. 2010; Schlaufman & Winn 2013; Stephan et al. 2018), which are still poorly understood. Furthermore, the increased irradiance on the planet caused by the evolution of the host star has been proposed as a means to distinguish between proposed mechanisms to explain the inflation of gas-giant planets beyond the limits expected from gravitational contraction and cooling (Hubbard et al. 2002; Lopez & Fortney 2016). Recent discoveries by the K2 mission have indeed yielded evidence that planets orbiting low-luminosity RGB stars are consistent with being inflated by the evolution of the host star (Grunblatt et al. 2016, 2017), favoring scenarios in which the energy from the star is deposited into the deep planetary interior (Bodenheimer et al. 2001).

Based on its radius and orbital period, TOI-197 would nominally be classified as a warm Saturn, sitting between the well-known population of hot Jupiters and the ubiquitous population of sub-Neptunes uncovered by Kepler (Figure 8a). Taking into account the evolutionary state of the host star, however, TOI-197 falls at the beginning of the "inflation sequence" in the radius-incident flux diagram (Figure 8b), with planet radius strongly increasing with stellar incident flux (Kovács et al. 2010; Demory & Seager 2011; Miller & Fortney 2011; Thorngren & Fortney 2018). Since TOI-197.01 is currently not anomalously large compared to the observed trend and scatter for similar planets (Figure 8b) and low-mass planets are expected to be more susceptible to planet reinflation (Lopez & Fortney 2016), TOI-197 may be a progenitor of a class of re-inflated gas-giant planets orbiting RGB stars.

If confirmed, the mild eccentricity of TOI-197.01 would be consistent with predictions of a population of planets around evolved stars for which orbital decay occurs faster than tidal circularization (Villaver et al. 2014; Grunblatt et al. 2018). Moreover, combining the asteroseismic age of the system with the possible non-zero eccentricity would allow constraints on the tidal dissipation in the planet, which drives the circularization of the orbit. Using the formalism by Mardling (2011) (see also Gizon et al. 2013; Davies et al. 2016; Ceillier et al. 2016), the current constraints would imply a minimum value of the planetary tidal quality factor $Q_{p;\min} \approx 3.2 \times 10^4$, below which the system would have been already circularized in $\sim 5\,\mathrm{Gyr}$. Compared to the
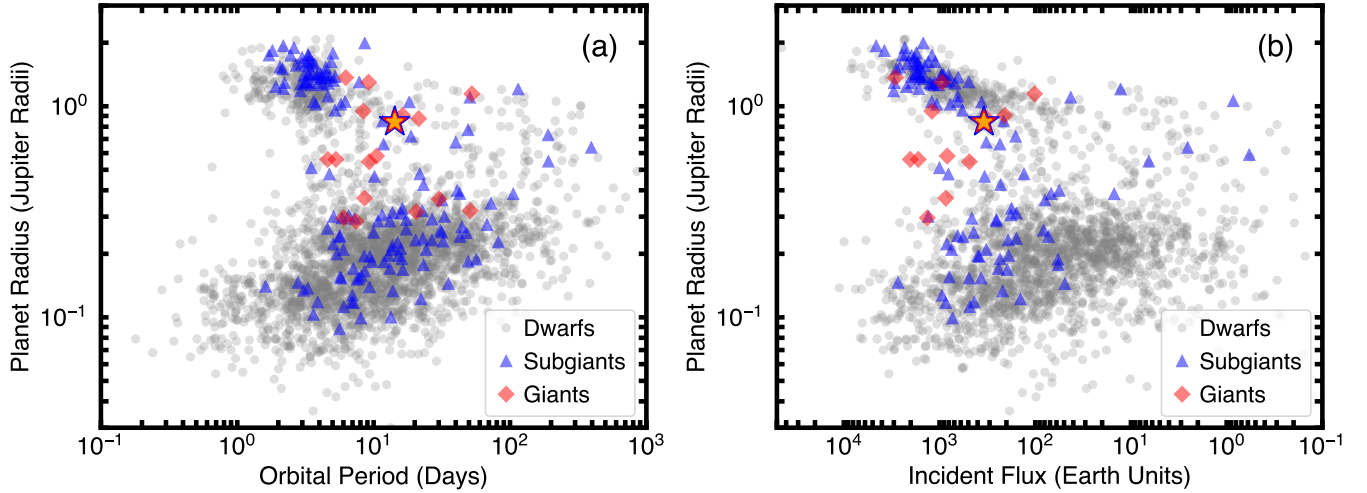
Figure 8. Planet radius versus orbital period (panel a) and incident flux (panel b) for confirmed exoplanets. Symbols are color-coded according to the evolutionary state of the host star (see Figure 7). TOI-197 b is highlighted in both panels with an orange/red/blue star symbol.

value measured in Saturn ($Q \approx 1800$, Lainey et al. 2017), this would demonstrate the broad diversity of dissipation observed in giant planets. Since tidal dissipation mechanisms vary strongly with internal structure (see e.g. Guenel et al. 2014; Ogilvie 2014; André et al. 2017), this may also contribute to understanding the internal composition of such planets. We caution, however, that further RV measurements will be needed to confirm a possible non-zero eccentricity for TOI-197.01.

The precise characterization of planets orbiting evolved, oscillating stars also provides valuable insights into the diversity of compositions of planets through their mean densities. TOI-197.01 falls in the transition region between Neptune and sub-Saturn sized planets for which radii increase as $R_P \approx M_P^{0.6}$, and Jovian planets for which radius is nearly constant with mass (Weiss et al. 2013; Chen & Kipping 2017, Figure 9). Recent studies of a population of sub-Saturns in the range ~ 4–$8\,R_\oplus$ also found a wide variety of masses, approximately 6–$60\,M_\oplus$, regardless of size (Petigura et al. 2017b; Van Eylen et al. 2018). Furthermore, masses of sub-Saturns correlate strongly with host star metallicity, suggesting that metal-rich disks form more massive planet cores. TOI-197.01 demonstrates that this trend does not appear to extend to planets with sizes $> 8\,R_\oplus$, given its mass of $\sim 60\,M_\oplus$ and a roughly sub-solar metallicity host star ([Fe/H] $\approx -0.08\,$dex). This suggests that Saturn-sized planets may follow a relatively narrow range of densities, a possible signature of the transition in the interior structure (such as the increased importance of electron degeneracy pressure, Zapolsky & Salpeter 1969) leading to different mass-
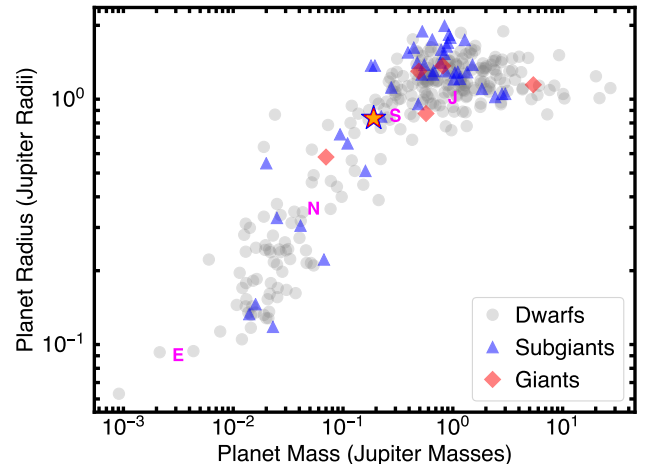
Figure 9. Mass-radius diagram for confirmed planets with densities measured to better than 50%. Symbols are color-coded according to the evolutionary state of the host star (see Figure 7). TOI-197 b is highlighted with a orange/red/blue star symbol. Magenta letters show the position of solar system planets.

radius relations between sub-Saturns and Jupiters. We note that TOI-197.01 is one of the most precisely characterized Saturn-sized planets to date, with a density uncertainty of $\sim 15\%$.

6. CONCLUSIONS

We have presented the discovery of TOI-197.01, the first transiting planet orbiting an oscillating host star identified by *TESS*. Our main conclusions are as follows:

- TOI-197 is a late subgiant / early red giant with a clear presence of mixed modes. Combined spectroscopy and asteroseismic modeling revealed that the star has just started its ascent on the red giant branch, with $R_\star = 2.943 \pm 0.064 R_\odot$, $M_\star = 1.212 \pm 0.074 M_\odot$ and near-solar age $(4.9 \pm 1.1 \, \mathrm{Gyr})$. TOI-197 is a typical oscillating star expected to be detected with *TESS*, and demonstrates the power of asteroseismology even with only 27 days of data.

- The oscillation amplitude of TOI-197 is consistent with ensemble measurements from *Kepler*. This confirms that the redder bandpass of *TESS* compared to *Kepler* only has a small effect on the oscillation amplitude (as expected from scaling relations, Kjeldsen & Bedding 1995; Ballot et al. 2011a), supporting the expected yield of thousands of solar-like oscillators with 2-minute cadence observations in the nominal *TESS* mission (Schofield et al. 2018). A detailed study of the asteroseismic performance of *TESS* will have to await ensemble measurements of noise levels and amplitudes.

- TOI-197.01 is a "hot Saturn" ($F = 343 \pm 24 F_\oplus$, $R_\mathrm{p} = 0.836 \pm 0.031 \, R_\mathrm{J}$, $M_\mathrm{p} = 0.190 \pm 0.018 \, M_\mathrm{J}$) and joins a small but growing population of close-in, transiting planets orbiting evolved stars. Based on its incident flux, radius and mass, TOI-197.01 may be a precursor to the population of gas giants that undergo radius re-inflation due to the increased irradiance as their host star evolves up the red-giant branch.

- TOI-197.01 is one the most precisely characterized Saturn-sized planets to date, with a density measured to $\sim 15\%$. TOI-197.01 does not follow the trend of increasing planet mass with host star metallicity discovered in sub-Saturns with sizes between $4-8 \, R_\oplus$, which has been linked to metal-rich disks preferentially forming more massive planet cores (Petigura et al. 2017b). The moderate density ($\rho_\mathrm{p} = 0.431 \pm 0.062 \, \mathrm{g \, cm^{-3}}$) suggests that Saturn-sized planets may follow a relatively narrow range of densities, a possible signature of the transition in the interior structure leading to different mass-radius relations for sub-Saturns and Jupiters.

TOI-197 provides a first glimpse at the strong potential of *TESS* to characterize exoplanets using asteroseismology. TOI-197.01 has one the most precisely characterized densities of known Saturn-sized planets to date,

with an uncertainty of $\sim 15\%$. Thanks to asteroseismology the planet density uncertainty is dominated by measurements of the transit depth and the radial velocity amplitude, and thus can be expected to further decrease with continued transit observations and radial velocity follow-up, which is readily performed given the brightness (V=8) of the star. Ensemble studies of such precisely characterized planets orbiting oscillating subgiants can be expected to yield significant new insights on the effects of stellar evolution on exoplanets, complementing current intensive efforts to characterize planets orbiting dwarfs.

REFERENCES

Allard, F., Homeier, D., & Freytag, B. 2012, Royal Society of London Philosophical Transactions Series A, 370, 2765, doi: 10.1098/rsta.2011.0269

André, Q., Barker, A. J., & Mathis, S. 2017, A&A, 605, A117, doi: 10.1051/0004-6361/201730765

Appourchaux, T., Chaplin, W. J., García, R. A., et al. 2012, A&A, 543, A54, doi: 10.1051/0004-6361/201218948

Astropy Collaboration, Price-Whelan, A. M., Sipőcz, B. M., et al. 2018, AJ, 156, 123, doi: 10.3847/1538-3881/aabc4f

Baglin, A., Auvergne, M., Boisnard, L., et al. 2006, in 36th COSPAR Scientific Assembly, Vol. 36, 3749

Ball, W. H., & Gizon, L. 2017, A&A, 600, A128, doi: 10.1051/0004-6361/201630260

Ballard, S., Chaplin, W. J., Charbonneau, D., et al. 2014, ApJ, 790, 12, doi: 10.1088/0004-637X/790/1/12

Ballot, J., Barban, C., & van't Veer-Menneret, C. 2011a, A&A, 531, 124, doi: 10.1051/0004-6361/201016230

Ballot, J., Gizon, L., Samadi, R., et al. 2011b, A&A, 530, A97, doi: 10.1051/0004-6361/201116547

Barclay, T. 2018, ktransit: Exoplanet transit modeling tool in python, Astrophysics Source Code Library. http://ascl.net/1807.028

Barclay, T., Rowe, J. F., Lissauer, J. J., et al. 2013, Nature, 494, 452, doi: 10.1038/nature11914

Bastien, F. A., Stassun, K. G., Basri, G., & Pepper, J. 2013, Nature, 500, 427, doi: 10.1038/nature12419

Basu, S., & Chaplin, W. J. 2017, Asteroseismic Data Analysis: Foundations and Techniques

Bazot, M., Vauclair, S., Bouchy, F., & Santos, N. C. 2005, A&A, 440, 615, doi: 10.1051/0004-6361:20052698

Bedding, T. R. 2012, in Astronomical Society of the Pacific Conference Series, Vol. 462, Progress in Solar/Stellar Physics with Helio- and Asteroseismology, ed. H. Shibahashi, M. Takata, & A. E. Lynas-Gray, 195

Bedding, T. R., Kjeldsen, H., Arentoft, T., et al. 2007, ApJ, 663, 1315, doi: 10.1086/518593

Bell, K. J., Hekker, S., & Kuszlewicz, J. S. 2019, MNRAS, 482, 616, doi: 10.1093/mnras/sty2731

Benomar, O., Baudin, F., Chaplin, W. J., Elsworth, Y., &
    Appourchaux, T. 2012, MNRAS, 420, 2178,
    doi: 10.1111/j.1365-2966.2011.20184.x

Benomar, O., Masuda, K., Shibahashi, H., & Suto, Y. 2014,
    PASJ, doi: 10.1093/pasj/psu069

Berger, T. A., Huber, D., Gaidos, E., & van Saders, J. L.
    2018, ApJ, 866, 99, doi: 10.3847/1538-4357/aada83

Bodenheimer, P., Lin, D. N. C., & Mardling, R. A. 2001,
    ApJ, 548, 466, doi: 10.1086/318667

Borucki, W. J., Koch, D., Basri, G., et al. 2010, Science,
    327, 977, doi: 10.1126/science.1185402

Bouchy, F., Bazot, M., Santos, N. C., Vauclair, S., &
    Sosnowska, D. 2005, A&A, 440, 609,
    doi: 10.1051/0004-6361:20052697

Bovy, J., Rix, H.-W., Green, G. M., Schlafly, E. F., &
    Finkbeiner, D. P. 2016, ApJ, 818, 130,
    doi: 10.3847/0004-637X/818/2/130

Brahm, R., Jordán, A., & Espinoza, N. 2017a, PASP, 129,
    034002, doi: 10.1088/1538-3873/aa5455

Brahm, R., Jordán, A., Hartman, J., & Bakos, G. 2017b,
    MNRAS, 467, 971, doi: 10.1093/mnras/stx144

Brahm, R., Espinoza, N., Jordán, A., et al. 2018, arXiv
    e-prints.   https://arxiv.org/abs/1811.02156

Bressan, A., Marigo, P., Girardi, L., et al. 2012, MNRAS,
    427, 127, doi: 10.1111/j.1365-2966.2012.21948.x

Buchhave, L. A., Latham, D. W., Johansen, A., et al. 2012,
    Nature, 486, 375, doi: 10.1038/nature11121

Bugnet, L., García, R. A., Davies, G. R., et al. 2018, A&A,
    620, A38, doi: 10.1051/0004-6361/201833106

Campante, T. L. 2018, Asteroseismology and Exoplanets:
    Listening to the Stars and Searching for New Worlds, 49,
    55, doi: 10.1007/978-3-319-59315-9_3

Campante, T. L., Lund, M. N., Kuszlewicz, J. S., et al.
    2016a, ApJ, 819, 85, doi: 10.3847/0004-637X/819/1/85

Campante, T. L., Schofield, M., Kuszlewicz, J. S., et al.
    2016b, ApJ, 830, 138, doi: 10.3847/0004-637X/830/2/138

Ceillier, T., van Saders, J., García, R. A., et al. 2016,
    MNRAS, 456, 119, doi: 10.1093/mnras/stv2622

Chaplin, W. J., Elsworth, Y., Davies, G. R., et al. 2014a,
    MNRAS, 445, 946, doi: 10.1093/mnras/stu1811

Chaplin, W. J., & Miglio, A. 2013, ARA&A, 51, 353,
    doi: 10.1146/annurev-astro-082812-140938

Chaplin, W. J., Basu, S., Huber, D., et al. 2014b, ApJS,
    210, 1, doi: 10.1088/0067-0049/210/1/1

Chen, J., & Kipping, D. 2017, ApJ, 834, 17,
    doi: 10.3847/1538-4357/834/1/17

Choi, J., Dotter, A., Conroy, C., et al. 2016, ApJ, 823, 102,
    doi: 10.3847/0004-637X/823/2/102

Chontos, A., Huber, D., Latham, D. W., et al. 2019, AJ, in
    press, arXiv:1903.01591.
    https://arxiv.org/abs/1903.01591

Christensen-Dalsgaard, J. 2008, Ap&SS, 316, 13,
    doi: 10.1007/s10509-007-9675-5

Ciardi, D. R., Beichman, C. A., Horch, E. P., & Howell,
    S. B. 2015, ApJ, 805, 16,
    doi: 10.1088/0004-637X/805/1/16

Claret, A., & Bloemen, S. 2011, A&A, 529, A75,
    doi: 10.1051/0004-6361/201116451

Corsaro, E., & De Ridder, J. 2014, A&A, 571, A71,
    doi: 10.1051/0004-6361/201424181

Corsaro, E., De Ridder, J., & García, R. A. 2015, A&A,
    579, A83, doi: 10.1051/0004-6361/201525895

Corsaro, E., Fröhlich, H.-E., Bonanno, A., et al. 2013,
    MNRAS, 430, 2313, doi: 10.1093/mnras/stt059

Corsaro, E., Mathur, S., García, R. A., et al. 2017, A&A,
    605, A3, doi: 10.1051/0004-6361/201731094

Creevey, O. L., Metcalfe, T. S., Schultheis, M., et al. 2017,
    A&A, 601, A67, doi: 10.1051/0004-6361/201629496

Cunha, M. S., Stello, D., Avelino, P. P.,
    Christensen-Dalsgaard, J., & Townsend, R. H. D. 2015,
    ApJ, 805, 127, doi: 10.1088/0004-637X/805/2/127

Davies, G. R., & Miglio, A. 2016, Astronomische
    Nachrichten, 337, 774, doi: 10.1002/asna.201612371

Davies, G. R., Silva Aguirre, V., Bedding, T. R., et al.
    2016, MNRAS, 456, 2183, doi: 10.1093/mnras/stv2593

Deheuvels, S., & Michel, E. 2011, A&A, 535, A91,
    doi: 10.1051/0004-6361/201117232

Demarque, P., Guenther, D. B., Li, L. H., Mazumdar, A., &
    Straka, C. W. 2008, Ap&SS, 316, 31,
    doi: 10.1007/s10509-007-9698-y

Demory, B.-O., & Seager, S. 2011, The Astrophysical
    Journal Supplement Series, 197, 12,
    doi: 10.1088/0067-0049/197/1/12

Eastman, J. 2017, EXOFASTv2: Generalized
    publication-quality exoplanet modeling code,
    Astrophysics Source Code Library.
    http://ascl.net/1710.003

Eastman, J., Gaudi, B. S., & Agol, E. 2013, PASP, 125, 83,
    doi: 10.1086/669497

Evans, D. W., Riello, M., De Angeli, F., et al. 2018, A&A,
    616, A4, doi: 10.1051/0004-6361/201832756

Fürész, G. 2008, PhD thesis, University of Szeged, Szeged,
    Hungary

Furlan, E., Ciardi, D. R., Everett, M. E., et al. 2017, AJ,
    153, 71, doi: 10.3847/1538-3881/153/2/71

García, R. A., Hekker, S., Stello, D., et al. 2011, MNRAS,
    414, L6, doi: 10.1111/j.1745-3933.2011.01042.x

García, R. A., Ceillier, T., Salabert, D., et al. 2014, A&A, 572, A34, doi: 10.1051/0004-6361/201423888

Gilbert, J., Bergmann, C., Bloxham, G., et al. 2018, in Society of Photo-Optical Instrumentation Engineers (SPIE) Conference Series, Vol. 10702, Ground-based and Airborne Instrumentation for Astronomy VII, 107020Y

Gilliland, R. L., McCullough, P. R., Nelan, E. P., et al. 2011, ApJ, 726, 2, doi: 10.1088/0004-637X/726/1/2

Gizon, L., Ballot, J., Michel, E., et al. 2013, Proceedings of the National Academy of Science, 110, 13267, doi: 10.1073/pnas.1303291110

Grec, G., Fossat, E., & Pomerantz, M. A. 1983, SoPh, 82, 55

Grunblatt, S. K., Huber, D., Gaidos, E. J., et al. 2016, AJ, 152, 185, doi: 10.3847/0004-6256/152/6/185

Grunblatt, S. K., Huber, D., Gaidos, E., et al. 2017, AJ, 154, 254, doi: 10.3847/1538-3881/aa932d

—. 2018, ApJL, 861, L5, doi: 10.3847/2041-8213/aacc67

Grundahl, F., Fredslund Andersen, M., Christensen-Dalsgaard, J., et al. 2017, ApJ, 836, 142, doi: 10.3847/1538-4357/836/1/142

Guenel, M., Mathis, S., & Remus, F. 2014, A&A, 566, L9, doi: 10.1051/0004-6361/201424010

Handberg, R., Brogaard, K., Miglio, A., et al. 2017, MNRAS, 472, 979, doi: 10.1093/mnras/stx1929

Handberg, R., & Campante, T. L. 2011, A&A, 527, A56, doi: 10.1051/0004-6361/201015451

Handberg, R., & Lund, M. N. 2014, MNRAS, 445, 2698, doi: 10.1093/mnras/stu1823

Hekker, S., Elsworth, Y., De Ridder, J., et al. 2011, A&A, 525, A131, doi: 10.1051/0004-6361/201015185

Høg, E., Fabricius, C., Makarov, V. V., et al. 2000, A&A, 355, L27

Hubbard, W. B., Burrows, A., & Lunine, J. I. 2002, ARA&A, 40, 103, doi: 10.1146/annurev.astro.40.060401.093917

Huber, D., Stello, D., Bedding, T. R., et al. 2009, Communications in Asteroseismology, 160, 74. https://arxiv.org/abs/0910.2764

Huber, D., Bedding, T. R., Arentoft, T., et al. 2011, ApJ, 731, 94, doi: 10.1088/0004-637X/731/2/94

Huber, D., Chaplin, W. J., Christensen-Dalsgaard, J., et al. 2013a, ApJ, 767, 127, doi: 10.1088/0004-637X/767/2/127

Huber, D., Carter, J. A., Barbieri, M., et al. 2013b, Science, 342, 331. https://arxiv.org/abs/1310.4503

Huber, D., Bryson, S. T., Haas, M. R., et al. 2017, ApJ, 224, 2, doi: 10.3847/0067-0049/224/1/2

Hunter, J. D. 2007, Computing In Science & Engineering, 9, 90, doi: 10.1109/MCSE.2007.55

Iben, Jr., I. 1965, ApJ, 142, 1447, doi: 10.1086/148429

Jenkins, J. M., Twicken, J. D., McCauliff, S., et al. 2016, in Proc. SPIE, Vol. 9913, Software and Cyberinfrastructure for Astronomy IV, 99133E

Johnson, J. A., Aller, K. M., Howard, A. W., & Crepp, J. R. 2010, PASP, 122, 905, doi: 10.1086/655775

Johnson, J. A., Petigura, E. A., Fulton, B. J., et al. 2017, AJ, 154, 108, doi: 10.3847/1538-3881/aa80e7

Jones, M. I., Brahm, R., Espinoza, N., et al. 2018, A&A, 613, A76, doi: 10.1051/0004-6361/201731478

Kallinger, T., Beck, P. G., Stello, D., & Garcia, R. A. 2018, A&A, 616, A104, doi: 10.1051/0004-6361/201832831

Kallinger, T., Hekker, S., Garcia, R. A., Huber, D., & Matthews, J. M. 2016, Science Advances, 2, 1500654, doi: 10.1126/sciadv.1500654

Kallinger, T., Hekker, S., Mosser, B., et al. 2012, A&A, 541, A51, doi: 10.1051/0004-6361/201218854

Kaufer, A., Stahl, O., Tubbesing, S., et al. 1999, The Messenger, 95, 8

Kjeldsen, H., & Bedding, T. R. 1995, A&A, 293, 87

Kjeldsen, H., Bedding, T. R., & Christensen-Dalsgaard, J. 2008a, ApJL, 683, L175, doi: 10.1086/591667

Kjeldsen, H., Bedding, T. R., Butler, R. P., et al. 2005, ApJ, 635, 1281, doi: 10.1086/497530

Kjeldsen, H., Bedding, T. R., Arentoft, T., et al. 2008b, ApJ, 682, 1370, doi: 10.1086/589142

Kovács, G., Bakos, G. Á., Hartman, J. D., et al. 2010, ApJ, 724, 866, doi: 10.1088/0004-637X/724/2/866

Lainey, V., Jacobson, R. A., Tajeddine, R., et al. 2017, Icarus, 281, 286, doi: 10.1016/j.icarus.2016.07.014

Lebreton, Y., & Goupil, M. J. 2014, A&A, 569, A21, doi: 10.1051/0004-6361/201423797

Lenz, P., & Breger, M. 2005, Communications in Asteroseismology, 146, 53, doi: 10.1553/cia146s53

Lopez, E. D., & Fortney, J. J. 2016, ApJ, 818, 4, doi: 10.3847/0004-637X/818/1/4

Lund, M. N., Handberg, R., Davies, G. R., Chaplin, W. J., & Jones, C. D. 2015, ApJ, 806, 30, doi: 10.1088/0004-637X/806/1/30

Lund, M. N., Handberg, R., Kjeldsen, H., Chaplin, W. J., & Christensen-Dalsgaard, J. 2017, in European Physical Journal Web of Conferences, Vol. 160, European Physical Journal Web of Conferences, 01005

Lund, M. N., Lundkvist, M., Silva Aguirre, V., et al. 2014, A&A, 570, A54, doi: 10.1051/0004-6361/201424326

Lundkvist, M. S. 2015, PhD thesis, Stellar Astrophysics Centre, Aarhus University, Denmark

Lundkvist, M. S., Kjeldsen, H., Albrecht, S., et al. 2016, Nature Communications, 7, 11201, doi: 10.1038/ncomms11201

Mann, A. W., Newton, E. R., Rizzuto, A. C., et al. 2016, AJ, 152, 61, doi: 10.3847/0004-6256/152/3/61

Mardling, R. A. 2011, in European Physical Journal Web of Conferences, Vol. 11, European Physical Journal Web of Conferences, 03002

Mathur, S., García, R. A., Régulo, C., et al. 2010, A&A, 511, A46, doi: 10.1051/0004-6361/200913266

Mathur, S., Hekker, S., Trampedach, R., et al. 2011, ApJ, 741, 119, doi: 10.1088/0004-637X/741/2/119

Mayor, M., Pepe, F., Queloz, D., et al. 2003, The Messenger, 114, 20

Miller, N., & Fortney, J. J. 2011, ApJL, 736, L29, doi: 10.1088/2041-8205/736/2/L29

Morel, P., & Lebreton, Y. 2008, Ap&SS, 316, 61, doi: 10.1007/s10509-007-9663-9

Mosser, B., Elsworth, Y., Hekker, S., et al. 2012a, A&A, 537, A30, doi: 10.1051/0004-6361/201117352

Mosser, B., Goupil, M. J., Belkacem, K., et al. 2012b, A&A, 548, A10, doi: 10.1051/0004-6361/201220106

Mosser, B., Benomar, O., Belkacem, K., et al. 2014, A&A, 572, L5, doi: 10.1051/0004-6361/201425039

Mosumgaard, J. R., Ball, W. H., Silva Aguirre, V., Weiss, A., & Christensen-Dalsgaard, J. 2018, MNRAS, 478, 5650, doi: 10.1093/mnras/sty1442

Nielsen, L. D., Bouchy, F., Turner, O., et al. 2019, A&A, 623, A100, doi: 10.1051/0004-6361/201834577

Ogilvie, G. I. 2014, ARA&A, 52, 171, doi: 10.1146/annurev-astro-081913-035941

Ong, J. M. J., & Basu, S. 2019, ApJ, 870, 41, doi: 10.3847/1538-4357/aaf1b5

Pande, D., Bedding, T. R., Huber, D., & Kjeldsen, H. 2018, MNRAS, 480, 467, doi: 10.1093/mnras/sty1869

Paxton, B., Bildsten, L., Dotter, A., et al. 2011, ApJS, 192, 3, doi: 10.1088/0067-0049/192/1/3

Paxton, B., Cantiello, M., Arras, P., et al. 2013, ApJS, 208, 4, doi: 10.1088/0067-0049/208/1/4

Paxton, B., Marchant, P., Schwab, J., et al. 2015, ApJS, 220, 15, doi: 10.1088/0067-0049/220/1/15

Pesnell, W. D. 1990, ApJ, 363, 227, doi: 10.1086/169333

Petigura, E. 2015, PhD Thesis, University of California. https://arxiv.org/abs/1510.03902

Petigura, E. A., Howard, A. W., Marcy, G. W., et al. 2017a, AJ, 154, 107, doi: 10.3847/1538-3881/aa80de

Petigura, E. A., Sinukoff, E., Lopez, E. D., et al. 2017b, AJ, 153, 142, doi: 10.3847/1538-3881/aa5ea5

Pires, S., Mathur, S., García, R. A., et al. 2015, A&A, 574, A18, doi: 10.1051/0004-6361/201322361

Queloz, D., Mayor, M., Udry, S., et al. 2001, The Messenger, 105, 1

Quinn, S. N., White, T. R., Latham, D. W., et al. 2015, ApJ, 803, 49, doi: 10.1088/0004-637X/803/2/49

Rayner, J., Bond, T., Bonnet, M., et al. 2012, in Proc. SPIE, Vol. 8446, Ground-based and Airborne Instrumentation for Astronomy IV, 84462C

Ricker, G. R., Winn, J. N., Vanderspek, R., et al. 2014, in Society of Photo-Optical Instrumentation Engineers (SPIE) Conference Series, Vol. 9143, , 20

Rodrigues, T. S., Girardi, L., Miglio, A., et al. 2014, MNRAS, 445, 2758, doi: 10.1093/mnras/stu1907

Rodrigues, T. S., Bossini, D., Miglio, A., et al. 2017, MNRAS, 467, 1433, doi: 10.1093/mnras/stx120

Roxburgh, I. W. 2017, A&A, 604, A42, doi: 10.1051/0004-6361/201731057

Schlaufman, K. C., & Winn, J. N. 2013, ApJ, 772, 143, doi: 10.1088/0004-637X/772/2/143

Schlegel, D. J., Finkbeiner, D. P., & Davis, M. 1998, ApJ, 500, 525, doi: 10.1086/305772

Schofield, M., Chaplin, W. J., Huber, D., et al. 2018, ApJS, submitted

Scuflaire, R., Montalbán, J., Théado, S., et al. 2008, Ap&SS, 316, 149, doi: 10.1007/s10509-007-9577-6

Serenelli, A., Johnson, J., Huber, D., et al. 2017, ApJS, 233, 23, doi: 10.3847/1538-4365/aa97df

Silva Aguirre, V., Davies, G. R., Basu, S., et al. 2015, MNRAS, 452, 2127, doi: 10.1093/mnras/stv1388

Skrutskie, M. F., Cutri, R. M., Stiening, R., et al. 2006, AJ, 131, 1163, doi: 10.1086/498708

Sliski, D. H., & Kipping, D. M. 2014, ApJ, 788, 148, doi: 10.1088/0004-637X/788/2/148

Smith, J. C., Stumpe, M. C., Van Cleve, J. E., et al. 2012, PASP, 124, 1000, doi: 10.1086/667697

Sousa, S. G. 2014, ARES + MOOG: A Practical Overview of an Equivalent Width (EW) Method to Derive Stellar Parameters, ed. E. Niemczura, B. Smalley, & W. Pych, 297–310

Sousa, S. G., Adibekyan, V., Delgado-Mena, E., et al. 2018, A&A, 620, A58, doi: 10.1051/0004-6361/201833350

Stassun, K. G., & Torres, G. 2016, AJ, 152, 180, doi: 10.3847/0004-6256/152/6/180

—. 2018, ApJ, 862, 61, doi: 10.3847/1538-4357/aacafc

Stassun, K. G., Oelkers, R. J., Pepper, J., et al. 2018, AJ, 156, 102, doi: 10.3847/1538-3881/aad050

Steffen, J. H., Ragozzine, D., Fabrycky, D. C., et al. 2012, Proceedings of the National Academy of Science, 109, 7982, doi: 10.1073/pnas.1120970109

Stello, D., Zinn, J., Elsworth, Y., et al. 2017, ApJ, 835, 83, doi: 10.3847/1538-4357/835/1/83

Stephan, A. P., Naoz, S., & Gaudi, B. S. 2018, AJ, 156, 128, doi: 10.3847/1538-3881/aad6e5

Stumpe, M. C., Smith, J. C., Catanzarite, J. H., et al. 2014, PASP, 126, 100, doi: 10.1086/674989

Tayar, J., & Pinsonneault, M. H. 2018, ApJ, 868, 150, doi: 10.3847/1538-4357/aae979

Tayar, J., Stassun, K. G., & Corsaro, E. 2018, arXiv e-prints. https://arxiv.org/abs/1812.04010

Thorngren, D. P., & Fortney, J. J. 2018, AJ, 155, 214, doi: 10.3847/1538-3881/aaba13

Tokovinin, A., Mason, B. D., & Hartkopf, W. I. 2010, AJ, 139, 743, doi: 10.1088/0004-6256/139/2/743

Torres, G., Fischer, D. A., Sozzetti, A., et al. 2012, ApJ, 757, 161, doi: 10.1088/0004-637X/757/2/161

Townsend, R. H. D., & Teitler, S. A. 2013, MNRAS, 435, 3406, doi: 10.1093/mnras/stt1533

Van Eylen, V., & Albrecht, S. 2015, ApJ, 808, 126, doi: 10.1088/0004-637X/808/2/126

Van Eylen, V., Dai, F., Mathur, S., et al. 2018, MNRAS, 478, 4866, doi: 10.1093/mnras/sty1390

Van Eylen, V., Albrecht, S., Huang, X., et al. 2019, AJ, 157, 61, doi: 10.3847/1538-3881/aaf22f

van Saders, J. L., Ceillier, T., Metcalfe, T. S., et al. 2016, Nature, 529, 181, doi: 10.1038/nature16168

van Saders, J. L., & Pinsonneault, M. H. 2013, ApJ, 776, 67, doi: 10.1088/0004-637X/776/2/67

Vanzi, L., Zapata, A., Flores, M., et al. 2018, MNRAS, 477, 5041, doi: 10.1093/mnras/sty936

Veras, D. 2016, Royal Society Open Science, 3, 150571, doi: 10.1098/rsos.150571

Verner, G. A., Elsworth, Y., Chaplin, W. J., et al. 2011, MNRAS, 415, 3539, doi: 10.1111/j.1365-2966.2011.18968.x

Villaver, E., Livio, M., Mustill, A. J., & Siess, L. 2014, ApJ, 794, 3, doi: 10.1088/0004-637X/794/1/3

Vogt, S. S., Allen, S. L., Bigelow, B. C., et al. 1994, in Society of Photo-Optical Instrumentation Engineers (SPIE) Conference Series, Vol. 2198, Society of Photo-Optical Instrumentation Engineers (SPIE) Conference Series, ed. D. L. Crawford & E. R. Craine, 362

Vrard, M., Mosser, B., Barban, C., et al. 2015, A&A, 579, A84, doi: 10.1051/0004-6361/201425064

Wang, S., Jones, M., Shporer, A., et al. 2019, AJ, 157, 51, doi: 10.3847/1538-3881/aaf1b7

Weiss, L. M., Marcy, G. W., Rowe, J. F., et al. 2013, ApJ, 768, 14, doi: 10.1088/0004-637X/768/1/14

Weiss, W. W., Moffat, A. F. J., & Kudelka, O. 2008, Communications in Asteroseismology, 157, 271

White, T. R., Bedding, T. R., Stello, D., et al. 2011, ApJ, 743, 161, doi: 10.1088/0004-637X/743/2/161

Wittenmyer, R. A., Endl, M., Wang, L., et al. 2011, ApJ, 743, 184, doi: 10.1088/0004-637X/743/2/184

Wizinowich, P., Acton, D. S., Shelton, C., et al. 2000, PASP, 112, 315, doi: 10.1086/316543

Wright, E. L., Eisenhardt, P. R. M., Mainzer, A. K., et al. 2010, AJ, 140, 1868, doi: 10.1088/0004-6256/140/6/1868

Yıldız, M., Çelik Orhan, Z., & Kayhan, C. 2016, MNRAS, 462, 1577, doi: 10.1093/mnras/stw1709

Yu, J., Huber, D., Bedding, T. R., & Stello, D. 2018, MNRAS, 480, L48, doi: 10.1093/mnrasl/sly123

Zapolsky, H. S., & Salpeter, E. E. 1969, ApJ, 158, 809, doi: 10.1086/150240